ORNL/NUREG/TM-10

Multirod Burst Test Program Quarterly Progress Report for October-December 1975

R. H. Chapman

OAK RIDGE NATIONAL LABORATORY
OPERATED BY UNION CARBIDE CORPORATION FOR THE ENERGY RESEARCH AND DEVELOPMENT ADMINISTRATION

Printed in the United States of America. Available from
National Technical Information Service
U.S. Department of Commerce
5285 Port Royal Road, Springfield, Virginia 22161
Price: Printed Copy $4.50; Microfiche $2.25

ORNL/NUREG/TM-10
NRC-1, -3

Contract No. W-7405-eng-26

MULTIROD BURST TEST PROGRAM
QUARTERLY PROGRESS REPORT FOR OCTOBER–DECEMBER 1975

R. H. Chapman

Work funded by the Nuclear Regulatory Commission
under Interagency Agreement 40-495-75

MAY 1976

OAK RIDGE NATIONAL LABORATORY
Oak Ridge, Tennessee 37830
operated by
UNION CARBIDE CORPORATION
for the
ENERGY RESEARCH AND DEVELOPMENT ADMINISTRATION

CONTENTS

PREFACE

The Multirod Burst Test (MRBT) program is being conducted in the Reactor Division of Oak Ridge National Laboratory for the Nuclear Regulatory Commission, Office of Nuclear Regulatory Research (NRC/ONRR); Dr. M. L. Picklesimer is the cognizant engineer for that organization.

Previously published MRBT progress reports are:

1. *Quarterly Progress Report on Reactor Safety Programs Sponsored by the Division of Reactor Safety Research for July–September 1974*, ORNL/TM-4729, Vol. I, pp. 70–72.

2. *Quarterly Progress Report on Reactor Safety Programs Sponsored by the NRC Division of Reactor Safety Research for October–December 1974*, ORNL/TM-4805, Vol. I, pp. 102–10.

3. *Quarterly Progress Report on Reactor Safety Programs Sponsored by the NRC Division of Reactor Safety Research for January–March 1975*, ORNL/TM-4914, Vol. I, pp. 78–104.

4. *Quarterly Progress Report on Reactor Safety Programs Sponsored by the NRC Division of Reactor Safety Research for April–June 1975*, ORNL/TM-5021, Vol. I, pp. 76–98.

5. R. H. Chapman, *Multirod Burst Test Program Quarterly Progress Report for July–September 1975*, ORNL/TM-5154.

SUMMARY

During this report period, prototypic simulators PS-10, PS-11, PS-13, and PS-16 were tested with SEMCO heater 2828005 and PS-12, PS-14, and PS-15 with SEMCO heater 2828006. All these tests were conducted from nominally the same initial conditions, except that a much higher initial pressure (12,920 vs ∿6500 kPa) was employed in PS-16 to investigate performance in this pressure range. Although a leak developed during the transient and the test was aborted, this test proved to be very interesting, in that failure occurred approximately 14 sec after termination of the transient.

With the exceptions of PS-11 and PS-13, the normal transient (i.e., termination of power at the time of rupture) followed by increased steam flow to effect rapid cooling, was employed for all these tests. The transient was modified for PS-11 to terminate power production at the instant deformation was observed (indicated by the pressure starting to decrease after having attained a maximum value), and the steam flow was increased with termination of the power transient to effect rapid cooling. In testing PS-13, power was terminated as in PS-11, but the steam flow was not increased to effect rapid cooling; this is the same transient used in testing PS-2, as reported last quarter. Although posttest deformation of PS-11 and PS-13 was not significantly different from other simulators tested with this heater, neither simulator burst.

The performance of simulators PS-10 (typical of the normal burst test), PS-11, PS-13, and PS-16 differed significantly, primarily due to the particular transient to which each was subjected. (The same heater was used in each of these simulators.) It would appear that any generalized deformation model for predicting ballooning of nuclear fuel rods should have the capability for modeling the general behavior observed for each of these simulators.

Simulators PS-12, PS-14, and PS-15 were tested with SEMCO heater 2828006. Prior to its use in these tests, the heater was grooved (for thermocouples) and plasma spray coated with a protective layer of ZrO_2. This was the first time these features were incorporated in the tests.

Pretest characterization (by infrared scanning) of the heater was performed after the grooving and coating operations. Surprising, none of these simulators burst in the high-temperature zone as indicated by the pretest infrared scan. Significant circumferential temperature variations were measured during the simulator tests.

Results from PS-10, PS-12, PS-14, and PS-15 (all tested with the normal test transient) were in agreement with previously reported tests conducted under nominally the same conditions.

SEMCO heater 2828005 was instrumented with thermocouples and tested in a bare heater configuration (i.e., without a cladding tube) to investigate temperature variations and lateral deflection resulting from circumferential temperature gradients. These tests confirmed the presence of axial gradients known to exist from heater infrared scans and posttest deformation profiles of simulators tested with this heater.

A procedure was developed and used successfully to spot weld thermocouples sheathed with nickel-plated stainless steel and tantalum inside the Zircaloy tubing. The procedure is based on the use of the special apparatus developed for this purpose.

Procedures were developed for pretreating the as-received Zircaloy tubing in superheated steam to produce a thin oxide film. Measurements on specimens from two pretreatment runs showed uniform thicknesses in the range of 0.5 to 1 μ.

Alternative methods for welding end adapters to the Zircaloy tubing were evaluated, and a method that employs a local shield with argon purging was selected. Although the method might result in some contamination in the weld zone, the economic savings are considered more than sufficient to justify its use.

Tests conducted on a model of a heated shroud for use with the 4 X 4 bundles indicate that the difference between the shroud temperature and the fuel pin simulators can be maintained within acceptable limits. The tests also provided important information on the type of thermocouple junction needed to separate the applied voltage (by the current carrying shroud) from the thermal emf induced in the junction by the ambient temperature.

Progress was made on fabrication of components for the multirod test facility. However, construction and assembly of the facility progressed slowly due to the checkout and test schedule of the Thermal-Hydraulic Test Facility (Blowdown Heat Transfer Program). This delay will not interfere with the Multirod Burst Test Program test schedule, since availability of the test bundle controls the test schedule.

As discussed previously, current-generation heaters have temperature variations that may make them very desirable for fuel pin simulators. However, characterization of the temperature distribution will be difficult but necessary to establish rupture temperatures and to permit determination of rod-to-rod interactions in the test arrays. Continued efforts to improve our infrared scanning techniques to demonstrate pretest characterization of circumferential temperature variations have been unsuccessful so far.

To date, we have received 30 heaters from SEMCO and 11 from RAMA, the 2 vendors with whom we have orders outstanding for 20 heaters. Of the 30 SEMCO heaters, 7 met the purchase order requirements, 7 were judged of potential use and were purchased for test purposes, and 10 were purchased at a reduced price for evaluation purposes. Of the 11 RAMA heaters, 2 met the purchase order requirements and 8 additional ones were purchased for heater evaluation purposes. We initiated action to exercise an option with SEMCO for 40 additional heaters for delivery at the earliest possible time.

1. INTRODUCTION

R. H. Chapman

The objectives of this program are to delineate the deformation behavior of unirradiated Zircaloy cladding under conditions postulated for a loss-of-coolant accident (LOCA) and to provide a data base to facilitate assessment of the magnitude and distribution of geometrical changes in the fuel rod cladding in a multirod array and of the extent of flow channel blockage that might result. Consistent and reliable data will be obtained from single- and multirod experiments that include possible effects of rod-to-rod interactions on ballooning and rupture behavior. These data will be used to (1) establish the magnitude and distribution of cladding deformation during temperature excursions representative of a hypothetical LOCA, (2) determine the cladding rupture temperature-pressure relationship, and (3) provide flow resistance information that can be related to the resultant coolant channel blockage.

Internally pressurized unirradiated Zircaloy tubes containing tubular electric heaters (to simulate nuclear fuel pellet heating) will be tested to failure in a low-pressure superheated-steam environment. These assemblies will be heated over a 915-mm (∿36-in.) length at a constant rate of 28°C/sec (50°F); differential pressures will range from about 700 to 14,000 kPa (100 to 2000 psi), corresponding to approximate rupture temperatures from 1200 to 700°C (2200 to 1300°F). In addition to measurements of cladding surface temperature and internal pressure during the transient test, data will be obtained on pre- and posttest flow resistance (for the multirod arrays) and on deformation, rupture strain, and channel blockage (as measured by sectioning of tubes and tube bundles).

Preliminary program plans and conceptual design descriptions were presented previously.[1] This report summarizes the progress made during the reporting period on design and construction of components and systems, development tests and evaluations, and procurement of long delivery items; and discusses preliminary results of single-rod tests.

2. PROGRAM PLANS AND ANALYSIS

2.1 Programmatic Activities

R. H. Chapman

Oak Ridge National Laboratory (ORNL) personnel (R. H. Chapman, G. G. Fee, R. E. MacPherson, and R. W. McCulloch) met with Reactor Safety Research (RSR) personnel (W. V. Johnston and M. L. Picklesimer) in Germantown in October to review preliminary single-rod burst test results and their implications for heater development and program schedules. These results indicate, for the conditions tested thus far, that cladding deformation is unusually sensitive to small variations in cladding temperature caused by similar variations in the surface temperature of the heater as reported in the previous report.[2] The results were discussed by Chapman in Germantown on October 10 at a meeting of the Nuclear Regulatory Commission, Office of Nuclear Regulatory Research (NRC/ONRR), Fuel Cladding Review Group and knowledgeable industry experts. Based on the comments of the participants, it appears that the temperature variations exhibited by the current generation of heaters are not too unlike those expected in nuclear fuel rods. If this is the case, tests conducted with these heaters may provide more realistic data on cladding deformation behavior. However, use of the heaters places extreme importance on pretest characterization of the temperature distribution to permit interpretation of the test results, which may prove to be more difficult than producing heaters of sufficient uniformity as to not require detailed characterization.

On December 2, E. D. Hindle, of the United Kingdom Atomic Energy Authority (UKAEA) Reactor Fuel Element Laboratories, visited ORNL for discussions on Zircaloy cladding behavior; details of the MRBT program and preliminary results from our single-rod tests were presented. The UKAEA group has conducted single-rod burst tests using resistance-heated tubes. Their results also indicate unusual deformation sensitivity to small temperature variations near the α-to-β transition.

In the MRBT program, reactor-grade Zircaloy-4 tubing is being tested out of reactor to determine its deformation behavior under transient conditions of temperature and pressure postulated to exist during a LOCA. As part of an extensive fuel behavior program, the Aerojet Nuclear Company (ANC) is investigating cladding deformation in a series of in-reactor experiments. Since the ANC investigation complements our studies, we have provided the ANC investigators with a complete set of drawings describing mechanical details of our bundle test arrays. Detailed discussions were held with J. R. Larson and E. E. Burdick (ANC) during their visit to ORNL on December 4 and 5. MRBT personnel will visit the ANC facilities next March or April to become more familiar with the details of their program.

Unanticipated technical difficulties encountered with procurement of heaters and small-diameter tantalum-sheathed thermocouples were evaluated with respect to their impact on programmatic objectives and schedules.

2.2 Preliminary Test Results

R. H. Chapman G. Hofmann*

A number of fuel pin simulators were fabricated and tested in a continuing effort to develop fabrication procedures, obtain preliminary test data to guide subsequent test activities, and evaluate heater performance. In addition, we are accumulating a data base on which the performance of prototype simulators can be judged. These data will augment those obtained later on simulators that include all the design features specified for the test program. The simulators were tested in a superheated-steam environment and examined as described in the previous report.[2]

Definition of the circumferential variation in temperature at selected locations was a major objective in a number of the simulator tests. Similarly, tests were performed on two heaters (SEMCO prototype heater 1 and SEMCO heater 2828005) in a bare heater configuration (i.e.,

*On assignment from Karlsruhe Nuclear Research Center.

without cladding) to obtain a direct measurement of the circumferential variations known to exist in these heaters.

Definition of the axial temperature variation (over selected short lengths) was studied in one series of simulator tests using SEMCO heater 2828006. This heater was grooved and plasma-spray coated with a protective layer of ZrO_2 prior to use.

Although considerable data were collected on magnetic tape for each of the tests conducted, recovery and analysis of the data are not yet automated, and only partial results can be presented at this time. These results will be grouped and discussed in the following sections according to the heater used in each test.

The Zircaloy tubes for all the simulators tested this quarter were obtained from the special lot of material purchased for this and other RSR test programs. Prior to fabrication into simulators, the tubes were pretreated in steam superheated to 482°C (900°F) for 30 min to produce a thin oxide film on the inside and outside surfaces.

Results of simulators tested with heater 2828005

The previous report[2] presented preliminary results obtained from tests of PS-8 and PS-9, using SEMCO heater 2828005. This heater was also used in a series of tests (PS-10, PS-11, and PS-13) this quarter to explore the effect of variations in the test conditions at the end of the power transient. The normal transient (i.e., termination of power at the time rupture occurs), followed by an increased steam flow to effect rapid cooling, was employed for PS-10 and was also used for testing PS-8 and PS-9. The transient was modified for PS-11 to terminate power production at the instant deformation was observed (indicated by the pressure starting to decrease after having attained a maximum value), and the steam flow was increased with termination of the power transient to effect rapid cooling. In testing PS-13, power was terminated as in PS-11, but the steam flow was not increased to effect rapid cooling; this is the same transient used in testing PS-2, as reported last quarter.[2]

The two significant findings from these tests were that PS-10 burst in the same vicinity as did PS-8 and PS-9 and that PS-11 and PS-13 did

not burst. The fact that PS-11 and PS-13 did not burst was surprising since PS-2, which was tested last quarter under similar conditions, did burst. These tests will be discussed in more detail in the following paragraphs.

Figure 2.1, which is made from a photograph of the data system cathode-ray tube (CRT) display, depicts the time dependence of several parameters measured during the test of PS-10. Although such plots are not particularly useful for detailed analysis, they are invaluable for

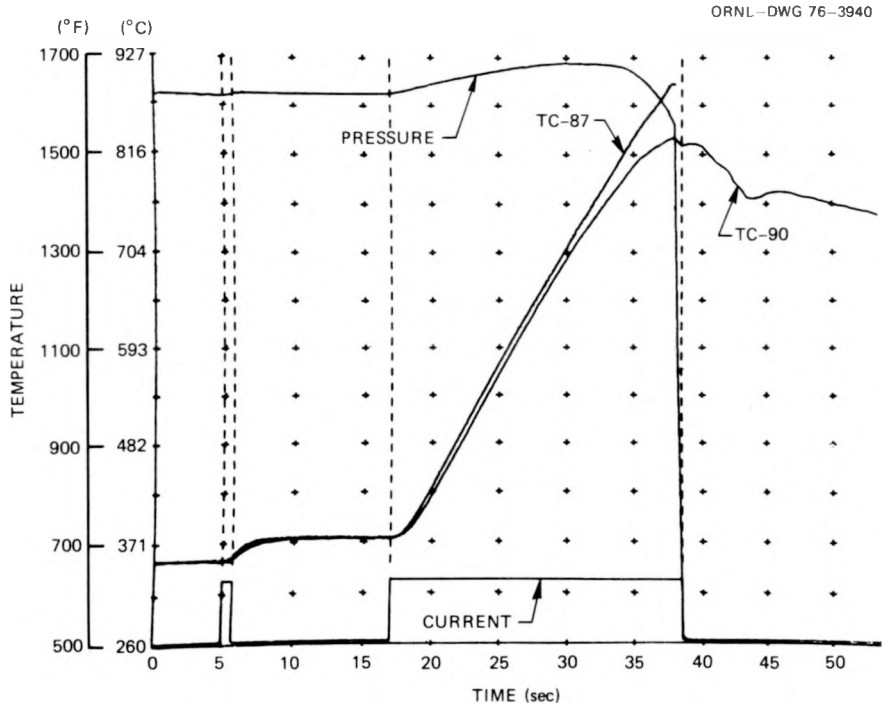

Thermocouple No.	Location of thermocouple	
	Distance above start of heated zone (cm)	Angular position (deg)
87	45.1	0
90	45.1	180

Fig. 2.1. Quick-look results of PS-10.

quick-look evaluations of the test results. A number of these plots are obtained after each test to permit immediate assessment of simulator performance. Detailed data tabulations and plots are obtained after these data are processed on the large computers.

Since a number of the quick-look data plots will be presented, it will be helpful to describe the features included in the figure. The abscissa is divided in 5-sec intervals, starting about 5 sec before power is applied to the heating element. The ordinate is divided into 55.6°C (100°F) intervals, starting at the 260°C (500°F) level. Electrical current, plotted as a step function in arbitrary units at the bottom of the graph, is used as a time mark for reference purposes, and dashed-line projections from the step changes in the current plot provide reference points for the other parameters. Pressure is plotted in arbitrary units as a smooth slowly varying curve near the top of the graph. Since the scale factor that is required to fit the pressure trace to the fixed temperature scale must be adjusted (internally by computer) to the appropriate value for locating the trace, the pressure scale is unavailable for the graphs. Selected thermocouple channel measurements are corrected [based on calibration data stored in the computer-controlled data-acquisition system (CCDAS)] and plotted as true values. Thermocouple identification and location data are tabulated in each of the figures.

Power to the test simulator is terminated manually by an operator observing a strip-chart recording of the pressure signal from a second transducer; the power-off switch is actuated as soon as the pressure undergoes a step change, indicating rupture. As evidenced by the quick-look plots, operator reaction time is in the order of 0.2 to 0.3 sec.

Figure 2.1 will now be used to describe the events that took place during testing of PS-10, including the behavior of thermocouples 87 and 90. Since one of the wires of TC-87 came unwelded immediately after the rupture, the plot for this channel was terminated at the time of burst. As indicated in the tabulation in the figure, TC-87 and TC-90 were located 180° apart at the same elevation. Thus, comparison of these channels provides information on the circumferential temperature variation at this particular axial position. Since rupture occurred slightly above the

point of attachment for TC-87, this channel provides a record of the temperature in the burst zone.

After thermal equilibration and pressurization of the simulator to the desired initial value, the power was turned on for less than a second to ascertain proper functioning of the instrumentation. This event, as indicated in Fig. 2.1 at t = 5 sec, was followed by about 10 to 12 sec of zero power operation to permit evaluation of the data scans. Upon initiation of the transient ($t \approx 17$ sec), the pressure responded almost immediately, while the thermocouples (on the outside surface of the Zircaloy tube) responded about 1 sec later. Comparing the temperature traces of the two thermocouples, one can see that a circumferential variation exists from the time the power is turned on and that the difference increases as the transient progresses. At the time of rupture, the difference was 60°C (108°F), which is consistent with the rupture occurring near the point where TC-87 was attached. The maximum measured temperature at burst was indicated by a thermocouple located about 7.6 cm (3 in.) above TC-87.

The maximum measured temperature in any given test is reported as the burst temperature; in general, the thermocouple indicating the maximum temperature is located in the vicinity of the burst. For example, in PS-10, the difference in the maximum measured temperature at burst [i.e., 901°C (1654°F)] and the temperature measured by TC-87 is only 5°C (9°F); this difference is considered insignificant in view of possible errors. Furthermore, the tube burst in the zone between these two thermocouples but very close to TC-87.

The axial location of the burst in PS-10 was between the failure points in PS-8 and PS-9, being about 8 mm ($\sim$0.32 in.) from the PS-8 failure point. Pertinent test results are summarized in Table 2.1, and Fig. 2.2 compares the posttest deformation of these three simulators.

A relative temperature profile of heater 2828005 obtained from a pretest infrared scan at 400°C (752°F) is also shown in Fig. 2.2. The maxima and minima in the deformation profiles for the three simulators are observed to correlate well with each other and with the pretest infrared scan. The failures occurred in a relatively flat temperature zone, as indicated by the infrared scan, and at essentially the same

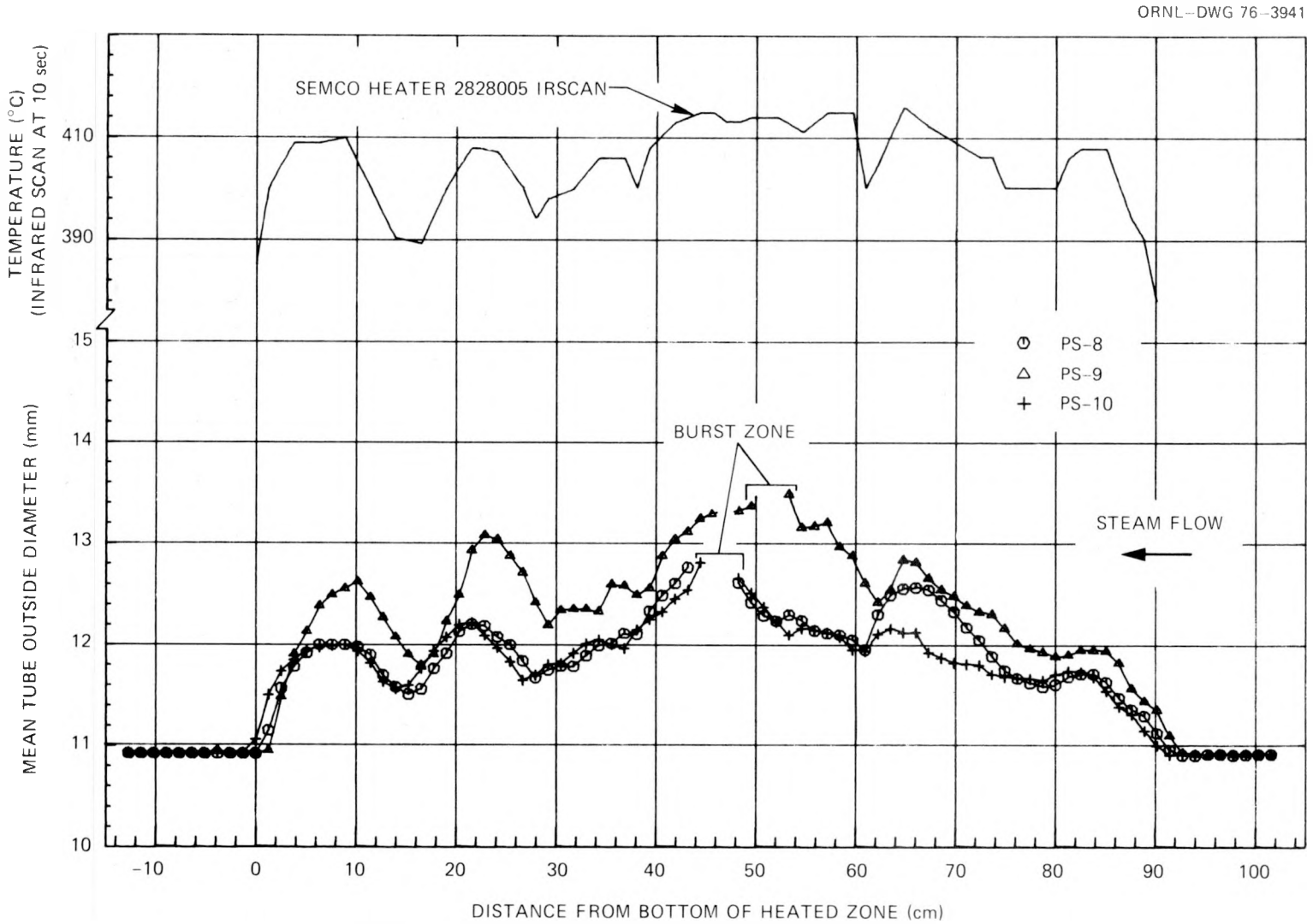

Fig. 2.2. Posttest deformation of PS-8, PS-9, and PS-10.

Table 2.1. Preliminary test results of simulators PS-8, PS-9, and PS-10

	PS-8	PS-9	PS-10
SEMCO heater No.	2828005	2828005	2828005
Measured gas volume,[a] cm^3 ($in.^3$)	30.6 (1.87)	35.6 (2.17)	35.9 (2.19)
Initial temperature, °C (°F)	349 (660)	346 (655)	352 (666)
Initial pressure, kPa (psi)	6470 (938)	6480 (940)	6440 (934)
Maximum pressure, kPa (psi)	6810 (988)	6890 (1000)	6830 (990)
Burst pressure, kPa (psi)	6000 (870)	5650 (820)	6000 (870)
Burst temperature,[b] °C (°F)	843 (1549)	866 (1591)	901 (1654)
Axial location of burst,[c] cm (in.)	45.1 (17.8)	50.2 (19.8)	45.9 (18.1)
Circumferential position,[d] deg	0	0	0
Time to rupture, sec	21.5	23.0	21.2
Rupture strain,[e] %	20	25	20

[a] At room temperature.

[b] Maximum measured temperature at time of rupture.

[c] Distance in elevation above lower limit of heated zone.

[d] Relative to heater position in PS-8.

[e] Obtained from tube outside perimeter from lip to lip of rupture.

circumferential position relative to the heater. This appears to be conclusive evidence that a significant circumferential temperature variation exists in the heater in this region, as measured in PS-10 (see Fig. 2.1). Circumferential measurements obtained from bare heater tests with this heater are discussed in a subsequent section.

As mentioned, SEMCO heater 2828005 was also used in the PS-11 assembly, and the power transient was terminated as soon as deformation was noted (by a pressure decrease following the maximum in the trace). Figure 2.3 shows a typical quick-look plot of this test. Initial test conditions for PS-11 were nominally the same as those for PS-10. Again, comparison of channels 87 and 90 (thermocouple locations are the same as in PS-10) shows a temperature variation around the circumference of the simulator, but it is much less than that observed in PS-10. Since the difference exists from the start of the test and does not appear to increase with time, it may be a result of the heater being located

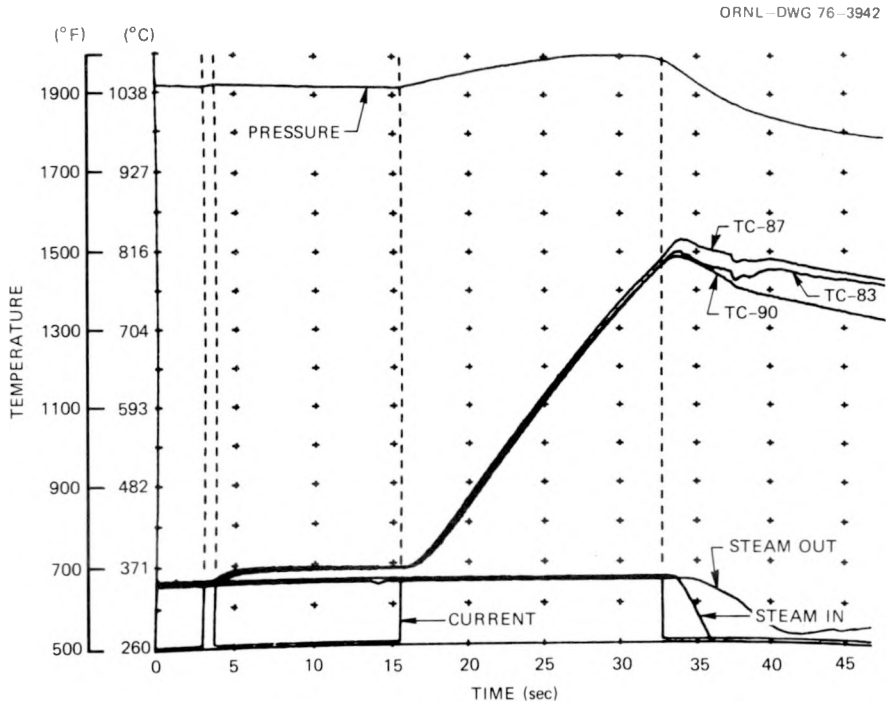

Thermocouple No.	Location of thermocouple	
	Distance above start of heated zone (cm)	Angular position (deg)
83	52.7	0
87	45.0	0
90	45.0	180

Fig. 2.3. Quick-look results of PS-11.

slightly eccentrically within the Zircaloy tube. Eccentric location of the heater may also be partly the cause of the large variation observed in PS-10.

As indicated by the current trace in Fig. 2.3, power input to the simulator was terminated as soon as deformation began. The combination of pressure loading and Zircaloy temperature and strength was such that considerable deformation occurred without actual rupture of the tube.

As indicated by the pressure trace in the figure, the pressure decayed exponentially with a long time constant.

Posttest deformation of PS-11 and PS-10 is compared in Fig. 2.4; excellent correspondence exists between the two simulators, and the deformation profiles correlate well with the relative temperature distribution as inferred from the heater pretest infrared scan. It should be noted that PS-11 deformation is almost identical to that of PS-10, even in the region where the latter failed. This provides evidence that the average circumferential strain in PS-10 was only slightly greater than the average strain in the unfailed simulator and also implies that PS-10 did not undergo generalized ballooning in the failure zone. On the contrary, significant ballooning occurred locally, that is, on the hot side of the simulator; large localized strains are expected to be found (in future examination) only in the immediate vicinity of the edges of the rupture zone. These observations appear to have an important bearing on the ballooning and subsequent flow blockage experienced by nuclear fuel rods; that is, axial and circumferential temperature distributions will tend to concentrate significant ballooning in highly localized hot spots on one side of the fuel rod. If this is the case, less flow blockage should result compared with the more or less symmetrical ballooning obtained with uniform temperature distribution.

Although steam inlet and outlet temperatures are plotted in Fig. 2.3, the outlet steam reading may have been influenced by the location of the thermocouple junctions; that is, the sensing junction may not have been responding to the flowing steam temperature. The sharp decrease in steam inlet temperature immediately after power termination is attributed to evaporation of moisture present in the (stagnant) steam bypass line before full-flow conditions are established through the bypass.

PS-13 test conditions (with SEMCO heater 2828005) were similar to those of PS-11, except that increased steam flow was prevented after the power was terminated. Quick-look results are given in Fig. 2.5, where the three thermocouple channels represent an axial temperature profile during the test. As in PS-11, the combination of pressure loading and Zircaloy temperature and strength caused significant deformation but did

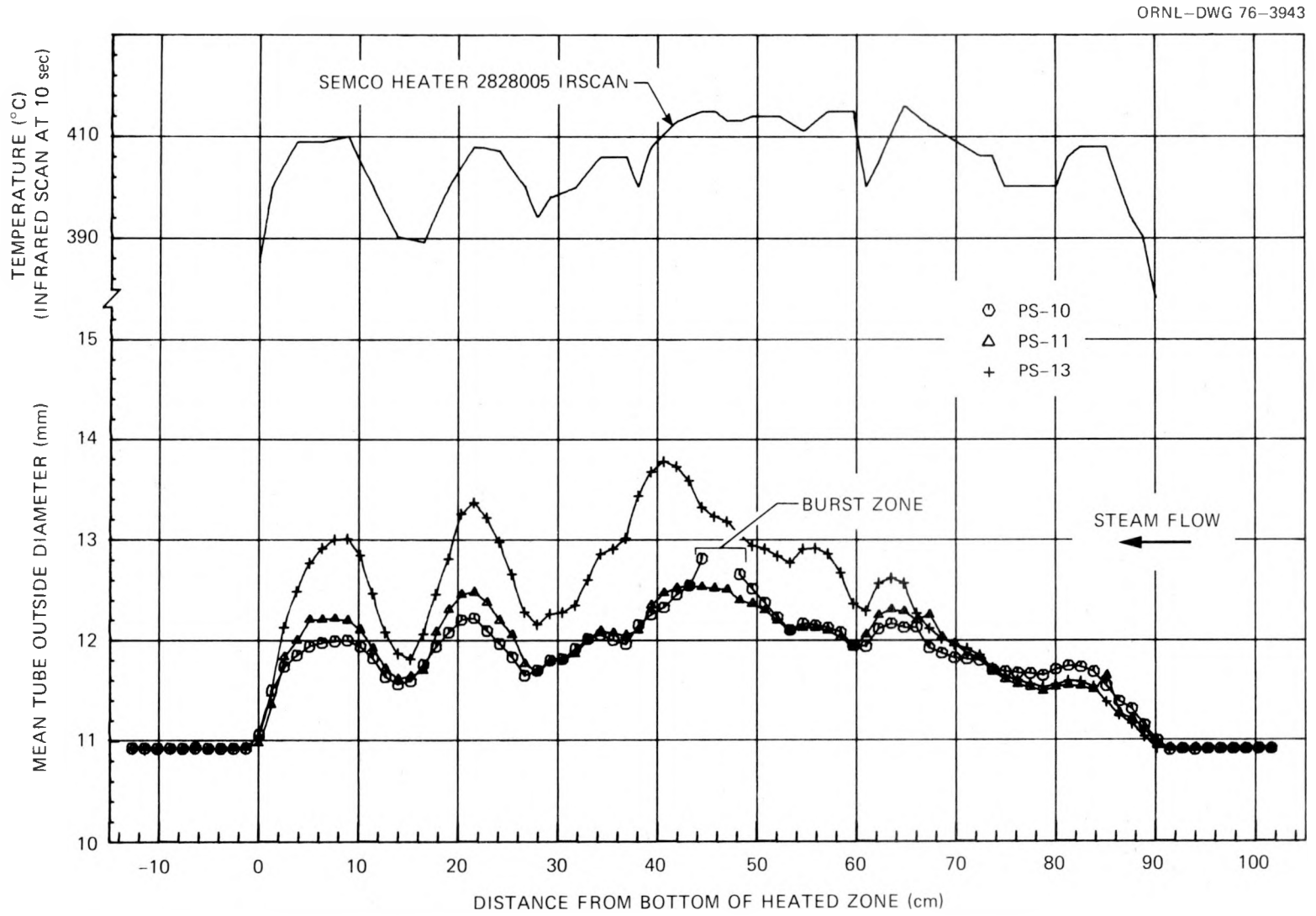

Fig. 2.4. Posttest deformation of PS-10, PS-11, and PS-13.

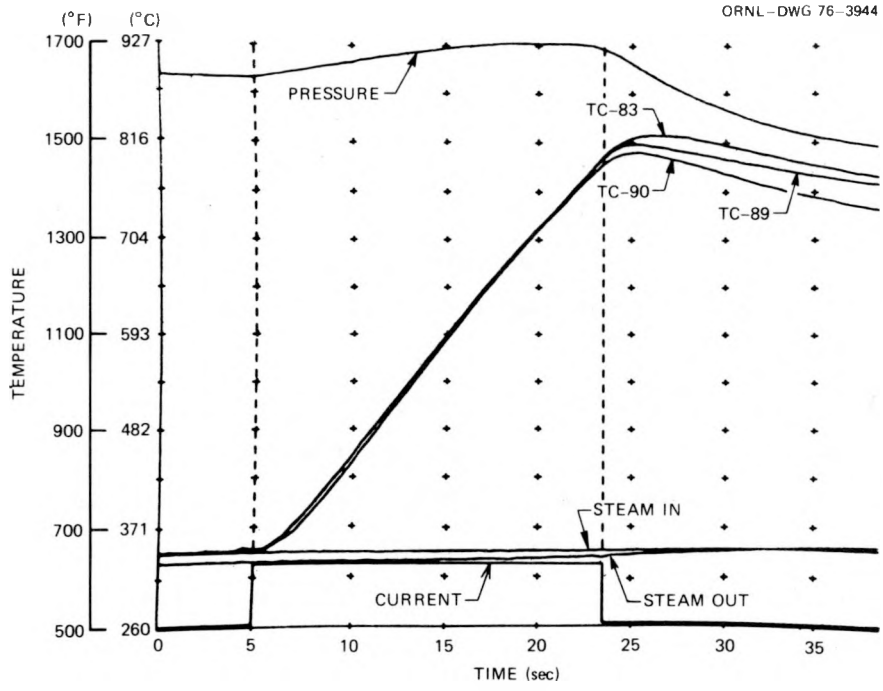

Thermocouple No.	Location of thermocouple	
	Distance above start of heated zone (cm)	Angular position (deg)
83	51.8	0
89	32.1	0
90	9.2	0

Fig. 2.5. Quick-look results of PS-13.

not cause rupture of the tube. Posttest deformation of PS-13 is compared with PS-10 and PS-11 results in Fig. 2.4. As indicated in the figure, PS-13 experienced somewhat greater deformation than did PS-11; this is attributed to the fact that PS-13 was subjected to higher pressure and temperature (due to the absence of posttest cooling steam) for a longer period of time than PS-11.

Simulators PS-8 through PS-11 and PS-13 were tested with SEMCO heater 2828005 starting from the same nominal conditions so that a maximum pressure of about 6895 kPa (1000 psi) would be experienced in the transient. The same heater was used to fabricate PS-16 for testing at a higher pressure, that is, 13,800 kPa (∿2000 psi). After thermal equilibration at 346°C (655°F), the simulator was pressurized with helium to 12,920 kPa (1875 psi) and isolated from the supply system; the initial gas volume was 37.8 cm^3 (2.31 $in.^3$).

Figure 2.6, which presents quick-look results of this unusual test, will be used to describe the sequence of events. For the first few seconds, the test progressed as expected, with the pressure and temperature increasing approximately linearly. After about 3 sec into the transient, the end seals apparently developed a leak, releasing the simulator pressure slowly and then rapidly to a level of about 9100 kPa (1320 psi). At this point, the elapsed time was about 8 sec; during this time the temperature increased uniformly, indicating that deformation was not the cause for the rapid depressurization. Also, the pressure leveled off for about 1 sec (indicating that the leak was arrested) and then slowly increased to a slightly higher value (as in a normal test) with increasing heatup. At about 14 sec into the transient, the pressure began to decrease in the manner normally attributed to deformation; the temperature at this time, as indicated by Fig. 2.6, was about 704°C (1300°F). The transient was terminated in the normal manner (i.e., with increased posttest steam cooling) by the operator after about 16.5 sec of power operation. The pressure continued to decrease during the cooldown cycle. If one compares this portion of the pressure trace with the pressure traces in Figs. 2.1 and 2.3, it can be seen that the decrease in pressure appears to be more characteristic of a reduction in temperature (see Fig. 2.3) than of increasing deformation (see Fig. 2.1). Finally, about 14 sec after termination of the power transient, the combination of pressure loading and Zircaloy temperature and strength were such as to cause the tube to burst. The burst occurred at a pressure of about 7350 kPa (1066 psi) and a temperature of 689°C (1272°F). These results should not be compared with the other burst test results,

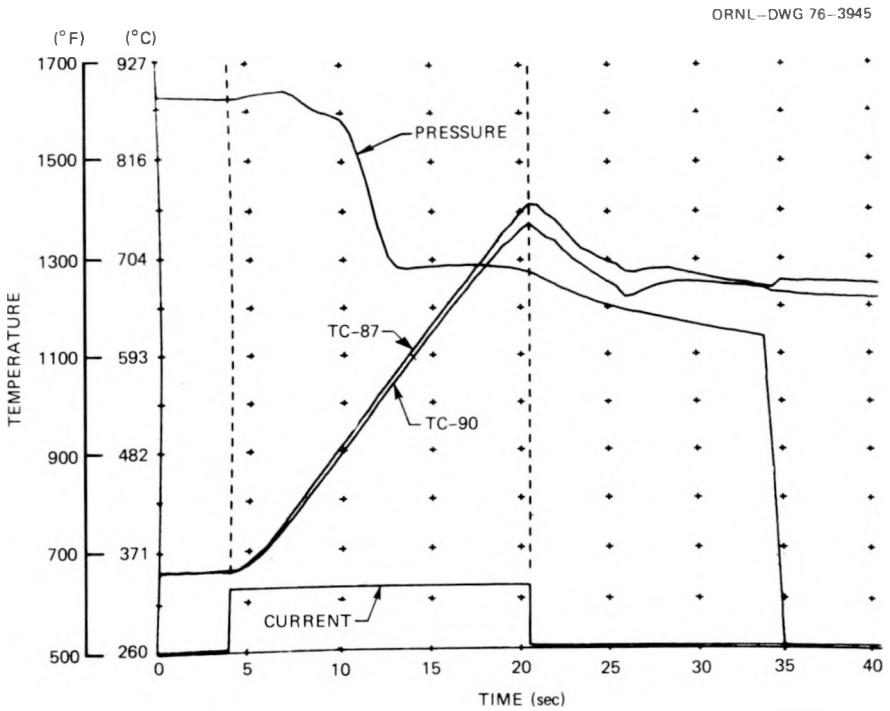

Thermocouple No.	Location of thermocouple	
	Distance above start of heated zone (cm)	Angular position (deg)
87	42.8	0
90	42.8	180

Fig. 2.6. Quick-look results of PS-16.

since the events leading up to the failure of PS-16 are not comparable to those normally encountered in the burst tests.

Posttest deformation of PS-16 is plotted in Fig. 2.7, with the heater pretest infrared temperature scan shown for reference. The deformation profile correlates with the infrared temperature distribution much the same as for previous simulators tested with this heater. The simulator burst (rupture strain of 28%) about 63 cm (24.8 in.) above the lower limit of the heated zone; previous bursts with this heater occurred

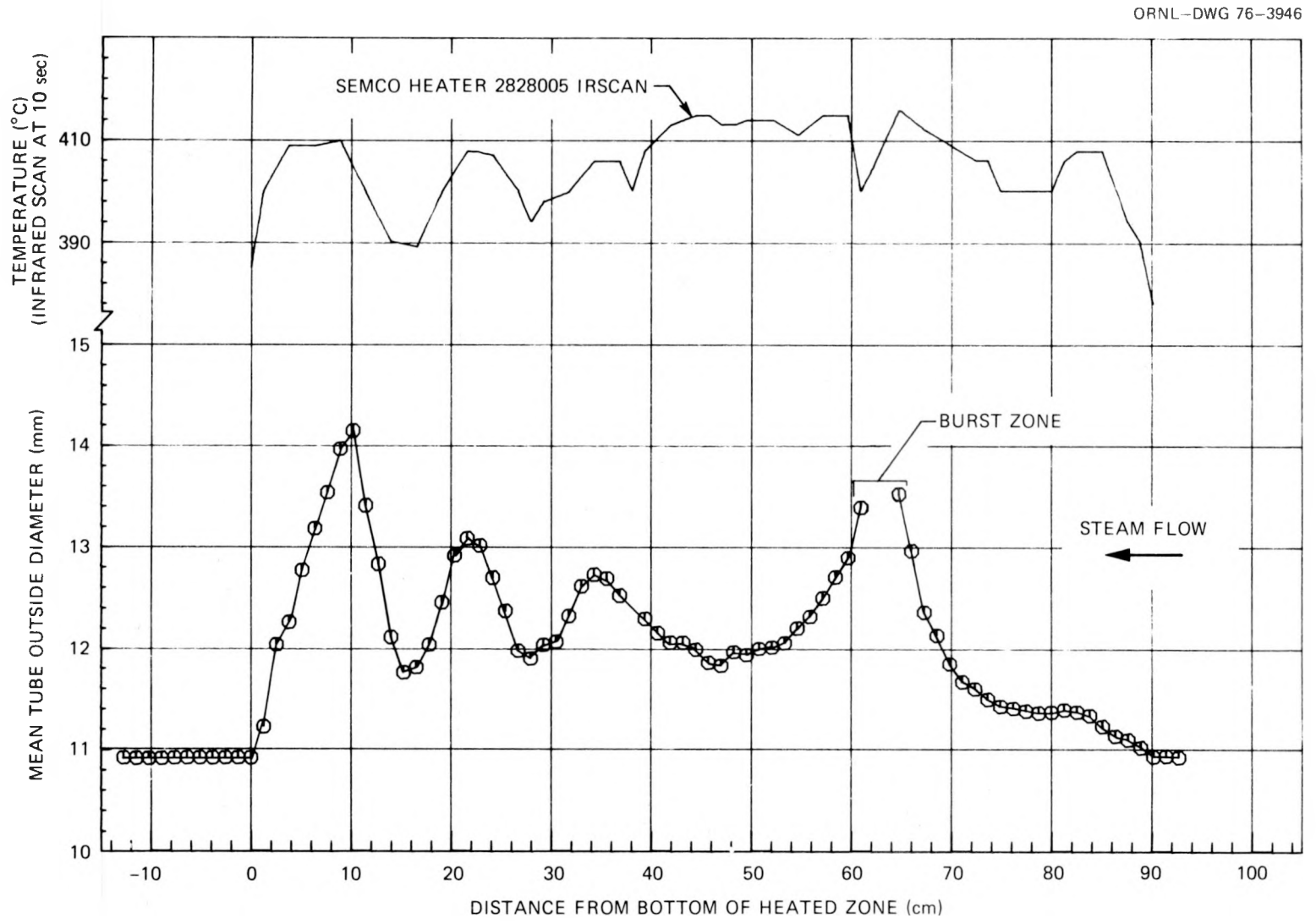

Fig. 2.7. Posttest deformation of PS-16.

in the relatively flat temperature region extending from 45 to 60 cm (17.7 to 23.6 in.) above the lower end of the heated zone (see Fig. 2.2). If one compares Fig. 2.4 with Fig. 2.7, it can be seen that deformation of PS-16 was slightly greater than that of PS-13, which did not burst.

It should be noted that the performance of simulators PS-10 (typical of the normal burst test), PS-11, PS-13, and PS-16 differed significantly, primarily due to the particular transient to which each was subjected. It would appear that any generalized deformation model for predicting ballooning of nuclear fuel rods should have the capability for modeling the general behavior observed for each of these simulators.

Results of simulators tested with heater 2828006

As reported last quarter,[2] SEMCO heater 2828006 was grooved and coated with a thin protective layer of ZrO_2 to evaluate the performance of simulators incorporating these features. Simulator PS-12 was fabricated with this heater, using four 0.75-mm-diam (0.030-in.) tantalum wires to model the internal thermocouples. Thirty-three external thermocouples were spot-welded to the outside of the Zircaloy tubing at selected spots in an attempt to obtain experimental verification of the temperature distribution inferred from the pretest infrared scan.

After thermal equilibration, the simulator was pressurized with helium to 6520 kPa (946 psi) at 340°C (644°F) and isolated from the supply system. Quick-look results are presented in Fig. 2.8. The maximum pressure encountered during the transient was 6900 kPa (1001 psi); the simulator burst at a pressure of about 6140 kPa (690 psi) and a temperature of 898°C (1648°F) as measured by thermocouple 49, which was located (fortuitously) in the immediate area of the burst. The outputs of two additional thermocouples (both located at the same elevation some distance above the burst point) are plotted in the figure for comparison. As can be observed, the circumferential variation in temperature as measured by channels 97 and 98 remained quite small throughout the test, although a significant difference was measured just before the burst. The temperature at the burst point, as measured by thermocouple 49, was significantly higher (throughout the test) than all the other measured

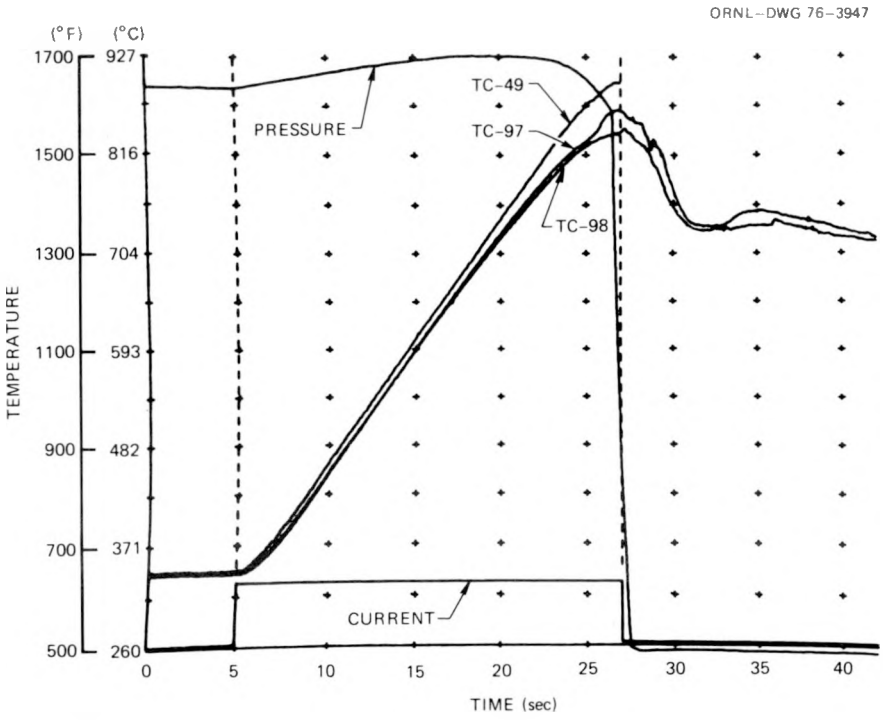

Thermocouple No.	Location of thermocouple	
	Distance above start of heated zone (cm)	Angular position (deg)
49	27.8	210
97	55.9	210
98	55.9	0

Fig. 2.8. Quick-look results of PS-12.

values, and, as indicated in Table 2.2, a large temperature difference (77°C) was measured around the tube at the time of failure.

Posttest deformation of PS-12 is plotted in Fig. 2.9, along with the temperature distribution of the grooved and coated heater, obtained by infrared scanning prior to fabrication of the simulator assembly, for reference. As with the previously tested simulators, the deformation of PS-12 agreed well with the infrared characterization of the heater. However, contrary to previous tests with other heaters, the simulator burst

Table 2.2. Comparison of measured temperatures (°C) around circumference of tube at two elevations in PS-12, PS-14, and PS-15 at time of burst

Simulator test	Transient time to burst (sec)	Cross section of highest temperature as indicated by pretest infrared scan[a]				Cross section at which failure occurred in PS-12[b]			
		0°	90°	180°	270°	0°	90°	180°	270°
PS-12	22.65	834	845	849	828	821	NA[c]	898[d]	NA[c]
PS-14	21.75	883	869	851	839	848	859	877	856
PS-15	20.95	832	885	847	817	839	837	866	862

[a]Thermocouples located 66 cm above bottom of heated zone.

[b]Thermocouples located 26.8 cm above bottom of heated zone.

[c]Thermocouples not installed at these positions in PS-12.

[d]Thermocouple located in immediate vicinity of burst.

in an average temperature zone, as indicated by the pretest infrared scan. This may have been the result of the heater being located eccentrically within the Zircaloy tube. (This situation can arise from dimensional tolerances and initial bowing of the heater.) Pertinent results of this test are given in Table 2.3.

The heater was recovered from the PS-12 simulator for reuse in PS-14. Visual examination of the plasma spray coating of ZrO_2 on the heater sheath revealed little damage, so the heater was straightened and reused in PS-14. Four tantalum wires were placed in the thermocouple grooves to center the heater within the Zircaloy tube. Since this test was planned to explore the reason why PS-12 burst in an unexpected (based on heater infrared characterization) region, only eight external thermocouples were employed (four at the cross section where PS-12 burst and four at the cross section indicated by the infrared scan to be hottest); see Table 2.2. Initial conditions for PS-14 were nominally the same as those used in testing PS-12; pertinent test parameters are given in Table 2.3. Quick-look results are given in Fig. 2.10, which includes temperature measurements for four points (90° apart) on the circumference of the Zircaloy tube near the point where failure occurred. A significant temperature variation existed at this cross section throughout the transient; the temperatures measured at the 0° (TC-83) and the 270° (TC-84) positions differed by approximately 50 to 60°C (90 to 108°F) during the deformation phase, with the 0° position indicating the highest temperature throughout the power transient. Temperature measurements around the tube at the time of burst are compared at the two instrumented cross sections and with PS-12 results in Table 2.2.

Posttest deformation of PS-14 is compared with PS-12 results in Fig. 2.9. As indicated in the figure, PS-14 deformation was similar to that of PS-12, being somewhat higher in the PS-14 rupture zone. Again, the rupture occurred in an unexpected location, based on the heater pretest infrared characterization.

The heater was recovered for use in PS-15. Since visual examination revealed that the ZrO_2 protective coating was in poor condition (powdery and easy to rub off), the coating was removed by brisk wiping with paper towels, leaving a very thin substrate of plasma-sprayed tantalum

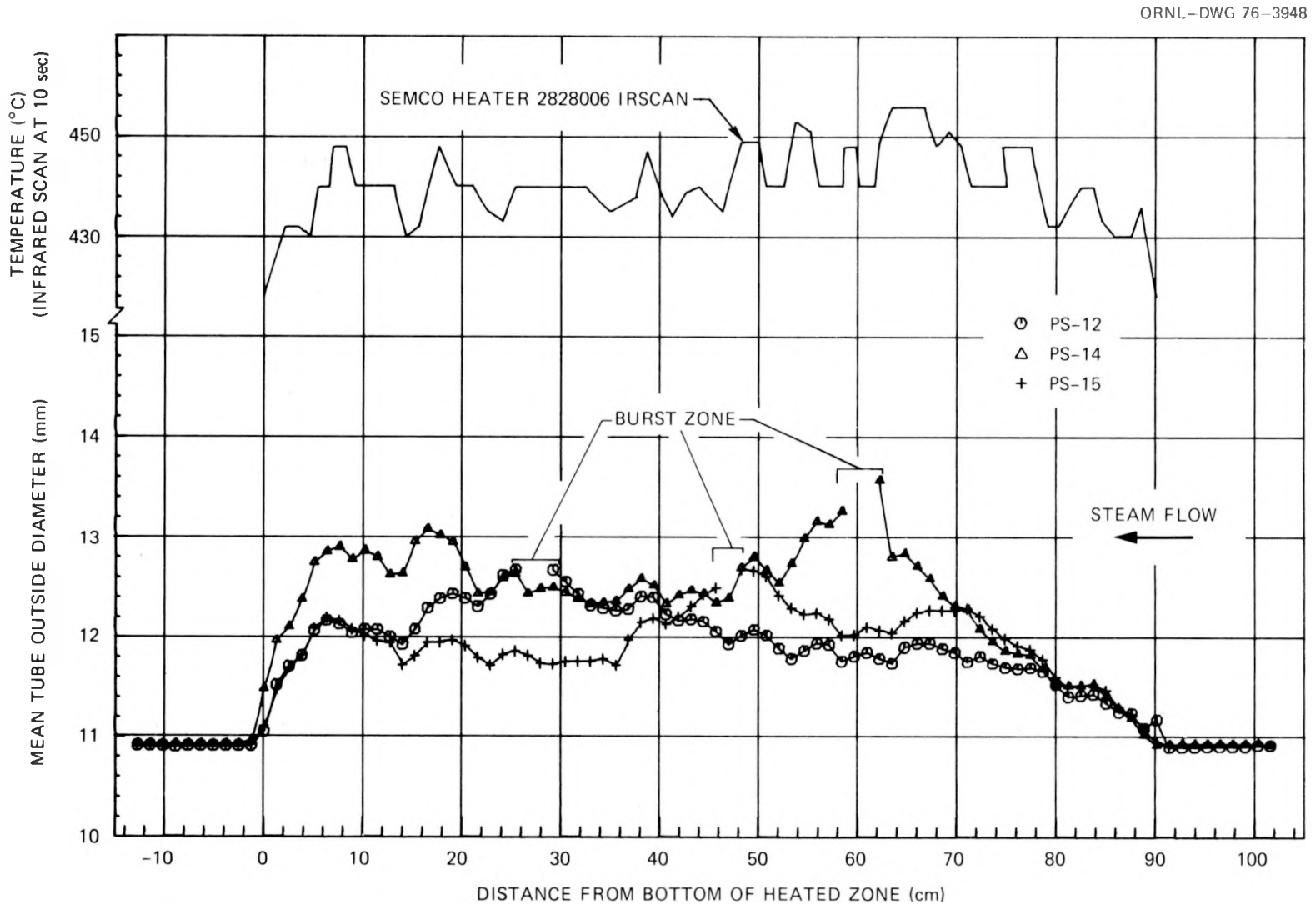

Fig. 2.9. Posttest deformation of PS-12, PS-14, and PS-15.

Table 2.3. Preliminary test results of simulators PS-12, PS-14, and PS-15

	PS-12	PS-14	PS-15
SEMCO heater No.	2828006	2828006	2828006
Measured gas volume,[a] cm^3 ($in.^3$)	41.0 (2.50)	41.5 (2.53)	46.9 (2.86)
Initial temperature, °C (°F)	340 (644)	337 (639)	352 (666)
Initial pressure, kPa (psi)	6520 (946)	6450 (935)	6490 (941)
Maximum pressure, kPa (psi)	6900 (1001)	6830 (991)	6780 (983)
Burst pressure, kPa (psi)	6140 (890)	5820 (844)	6160 (893)
Burst temperature,[b] °C (°F)	898 (1648)	883 (1621)	885 (1625)
Axial location of burst,[c] cm (in.)	27.3 (10.8)	60.0 (23.6)	47.6 (18.8)
Circumferential position,[d] deg	180	10	30
Time to rupture, sec	21.75	22.65	20.95
Rupture strain,[e] %	18	25	17

[a] At room temperature.

[b] Maximum measured temperature at time of rupture.

[c] Distance in elevation above lower limit of heated zone.

[d] Relative to arbitrary zero reference on heater.

[e] Obtained from tube outside perimeter from lip to lip of rupture.

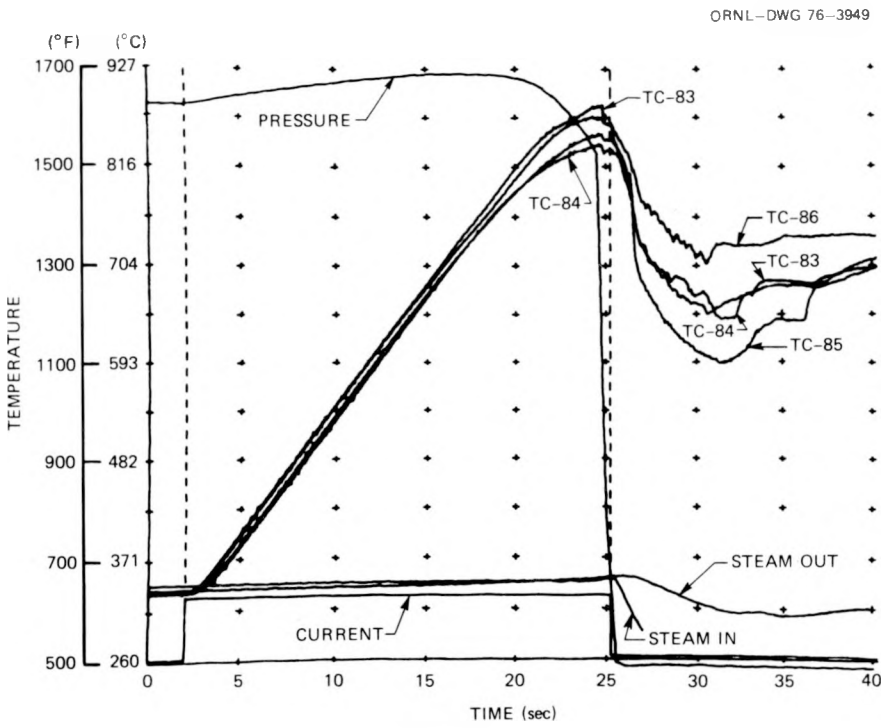

Thermocouple No.	Location of thermocouple	
	Distance above start of heated zone (cm)	Angular position (deg)
83	66	0
86	66	90
85	66	180
84	66	270

Fig. 2.10. Quick-look results of PS-14.

(applied to the stainless steel surface to obtain better adherence of the ZrO_2). Simulator PS-15 was assembled with four type K thermocouples (two with tantalum sheaths and two with stainless steel sheaths) spot-welded to the inside surface of the Zircaloy tube; this was the first simulator to incorporate internal thermocouples. (One of the tantalum-sheathed thermocouples was damaged during subsequent assembly operations

and was not available for use in the test.) The internal thermocouples were located at the axial position where the PS-12 tube failed; four bare-wire thermocouples were spot welded to the outside of the tube at the same positions as the internal thermocouples. In addition, four external thermocouples were equally spaced around the tube at the cross section where PS-14 burst and four at the cross section indicated by the infrared scan to be the hottest.

Initial conditions for the PS-15 test were nominally the same as for the other two tests (PS-12 and PS-14) in which SEMCO heater 2828006 was used. Typical quick-look results are plotted in Fig. 2.11. The temperature measurements plotted in the figure were obtained from the tantalum-sheathed internal thermocouple (channel 74) and the mating external thermocouple (channel 91). Posttest radiographs revealed that the external thermocouple was not positioned exactly over the internal thermocouple. Although the results have not been analyzed in detail, the general trends exhibited by these measurements are as would be expected.

Posttest deformation of PS-15 is plotted in Fig. 2.9 for comparison with PS-12 and PS-14. As can be seen in the figure, PS-15 burst in a different location. Temperatures measured around the tube at the time of failure are compared in Table 2.2 with the other tests conducted with this heater. Similarly, Table 2.3 compares the test results.

Burst tests on simulators using SEMCO prototype heaters 1 and 2 and with SEMCO heater 2828005 all gave reasonable correlation between the burst location and the heater hot spot as inferred from the pretest infrared temperature characterization. On the other hand, none of the three simulators tested with SEMCO heater 2828006 burst in the zone indicated by the infrared characterization to be the hottest. This may be the result of eccentric location of the heater within the Zircaloy tube and/or the inability of the infrared scan to define the temperature profile adequately for this purpose. It should be pointed out that heater 2828006 was scanned after it was grooved and coated with ZrO_2, and the infrared scans may not have been interpreted properly; we plan to scan the heater again to determine if this is the case. These results indicate the difficulty of locating internal thermocouples in the suspected failure zone on the basis of pretest infrared characterization of heaters.

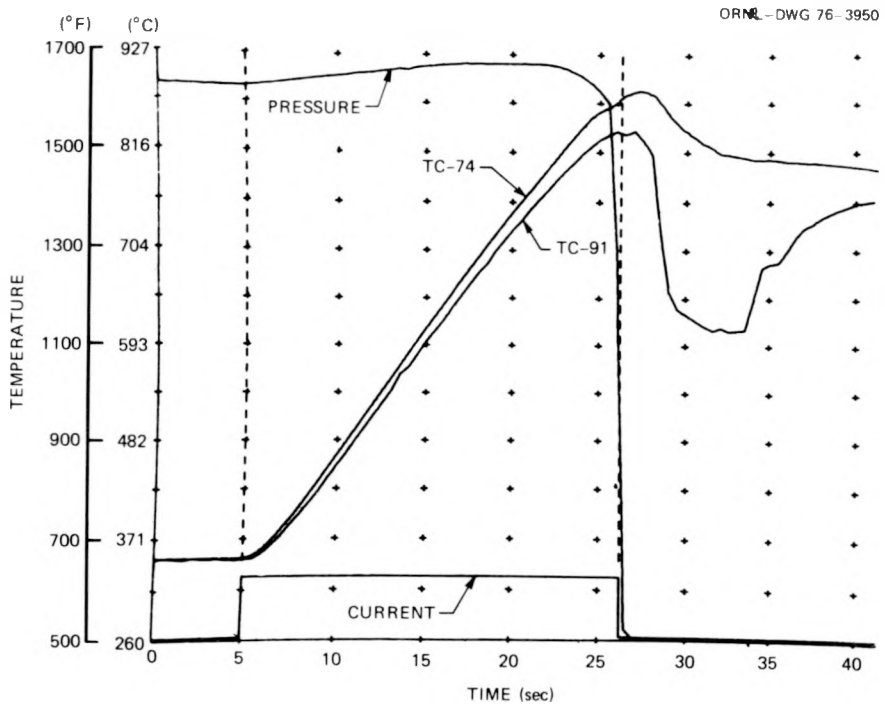

Thermocouple No.	Location of thermocouple	
	Distance above start of heated zone (cm)	Angular position (deg)
74 (internal)	26.8	330
91 (external)	27.3	330

Fig. 2.11. Quick-look results of PS-15.

The ability to position thermocouples in the desired location on the basis of the pretest characterization is particularly important for the bundle simulators.

Results of bare heater tests with heater 2828005

Three simulators using SEMCO heater 2828005 burst in essentially the same location relative to the heater (see Fig. 2.2), and the deformation profiles of two simulators that did not burst corresponded to the

profiles of simulators that did (see Fig. 2.4). This behavior strongly suggests the presence of significant temperature gradients (axially and circumferentially) in the heater. So far, we have been unable to discern circumferential gradients in the suspected zone using the high-temperature infrared scanning technique. (We are continuing our efforts to improve this capability.) Experimental verification of the suspected gradients was sought in a series of bare heater tests by direct measurement with bare-wire thermocouples spot welded to the heater sheath. Figure 2.12 gives the thermocouple identifications and locations relative to the infrared characterization of the heater. The thermocouples were attached to the heater in the relatively flat temperature zone (cross

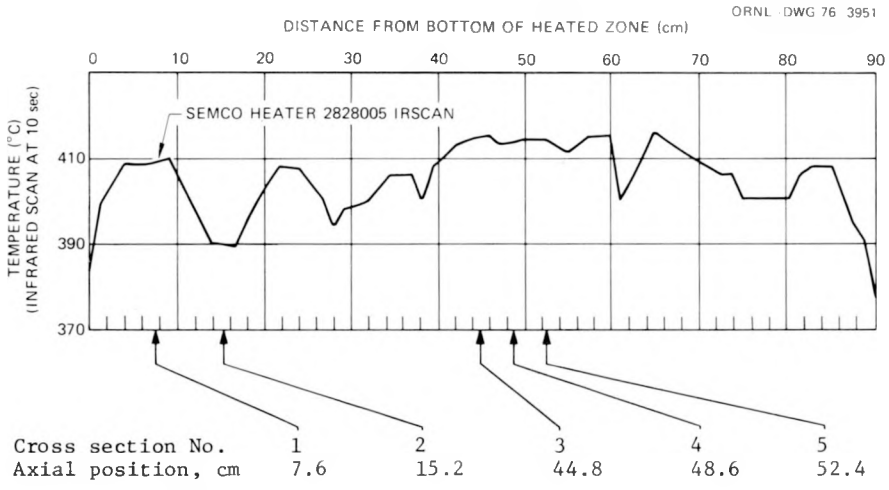

Test No.	Angular Location (deg)	Thermocouple No.				
1	0	TC 95	TC 93	TC 87	TC 86	TC 83
	90	TC 85			TC 91	
	180	TC 98	TC 94	TC 90	TC 89	TC 88
	270	TC 97			TC 92	
2	0	TC 98		TC 87	TC 86	
	90	TC 97			TC 91	
	180	TC 95		TC 90	TC 89	
	270	TC 85			TC 92	

Fig. 2.12. Thermocouple identifications and locations in bare heater tests with SEMCO heater 2828005.

sections 3, 4, and 5 in Fig. 2.12) where tube bursts had occurred (see Fig. 2.2) and in zones (cross sections 1 and 2 in Fig. 2.12) where large axial temperature gradients might be expected, based on the infrared scan.

The heater (without a Zircaloy tube) was suspended vertically in an 80-mm-ID (3.15-in.) quartz tube open at the top. The support permitted free downward expansion and lateral bowing of the heater during the heatup cycle. A small argon purge (up-flow) was maintained through the quartz tube during the tests.

Chronologically, test 1 was conducted on the heater following its use in simulators PS-8 through PS-11; test 2 was conducted following use of the heater in PS-13 and before its use in PS-16. This chronology may may be of importance in explaining heater performance in these and subsequent simulator tests conducted with this heater. In test 1, the heater was ramped several times to approximately 900°C (1652°F), with data being recorded during two of the runs; these ramps were then followed by two ramps to about 1160°C (2120°F), with data being recorded on each run. Later (after use of the heater in PS-13) the bare heater test configuration was reassembled for test 2, with thermocouples located as indicated in Fig. 2.12. The same test schedule was used in test 2 (low-temperature ramps followed by high-temperature ramps) as was used for test 1. Quick-look results of runs 1 and 2 of test 1 are shown in Figs. 2.13 and 2.14 respectively.

These quick-look plots are similar to those previously shown for simulator tests. The square-wave function plotted near the horizontal axis represents power on and power off; the "rough" square-wave function (obtained from current data) plotted near the upper limit of the graph is an artifact used to recover the data and should be ignored. Both figures show the temperature measured at the 0 and 180° positions at cross section 3 (Fig. 2.12), that is, at the approximate location of bursts in PS-8 and PS-10.

Table 2.4 presents a summary of the differences measured at approximately the same general temperature level in each of the tests. The temperature level selected for presentation of the tabulated data is approximately the burst temperature for the simulators tested thus far.

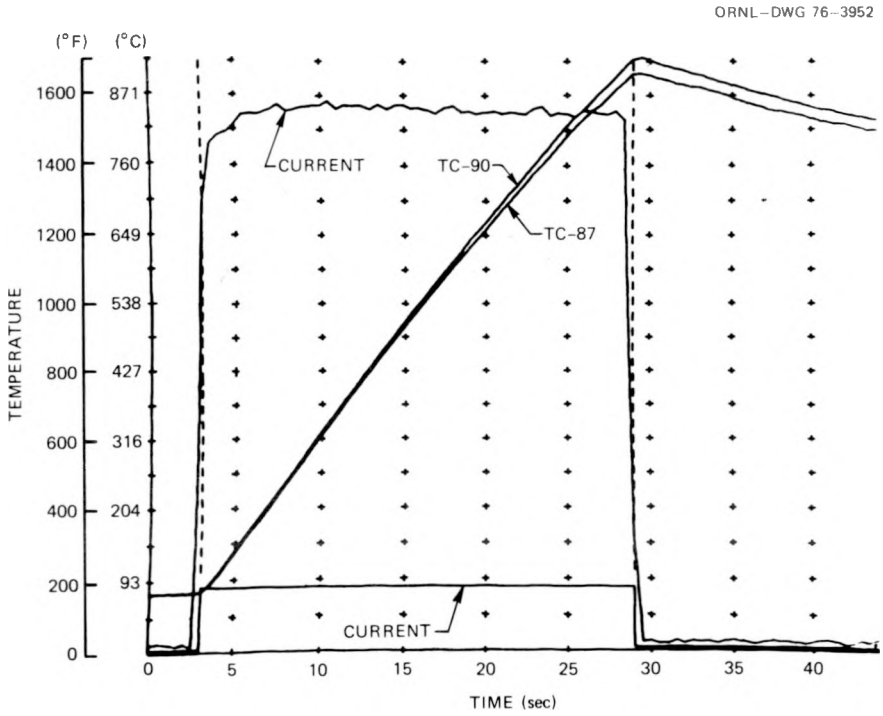

Thermocouple No.	Location of thermocouple	
	Distance above start of heated zone (cm)	Angular position (deg)
87	44.8	0
90	44.6	180

Fig. 2.13. Quick-look results of bare heater test 1, run 1, using SEMCO heater 2828005.

Since the axial and circumferential differences generally increase with increasing temperature, the values reported in the table are inappropriate for other temperature levels. The circumferential differences at a given cross section are consistent between runs 1 and 2 of a given test series but are not necessarily consistent between the two test series.

The steep axial temperature gradient between cross sections 1 and 2 indicated by the infrared scan (see Fig. 2.12) was confirmed by the thermocouple measurements. At a general temperature level corresponding to

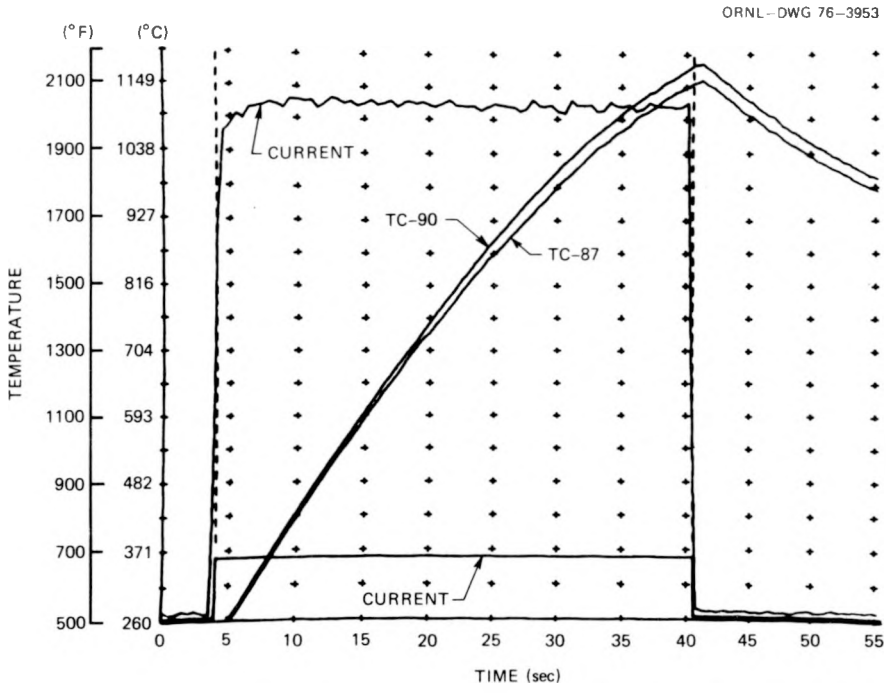

Thermocouple No.	Location of thermocouple	
	Distance above start of heated zone (cm)	Angular position (deg)
87	44.8	0
90	44.6	180

Fig. 2.14. Quick-look results of bare heater test 1, run 2, using SEMCO heater 2828005.

the infrared scan (∿400°C), all the measurements agreed well with the scan results. However, the gradient increased with increasing temperature. Similarly, the relatively flat temperature zone indicated by the scan (cross sections 3 to 5 in Fig. 2.12) was also indicated by the thermocouple measurements, although circumferential variations (see Table 2.4) confuse the relationship between the thermocouple measurements

Table 2.4. Measured temperature differences in bare heater tests with SEMCO heater 2828005

Test	Temperature[a] (°C)	Maximum measured[b] temperature difference (°C)	Maximum measured circumferential temperature difference at cross sections shown in Fig. 2.12 (°C)				
			1	2	3	4	5
Test 1, run 1	870	42	2	7	24	18	3
Test 1, run 2	845	36	9	10	23	16	NA[c]
Test 2, run 1	870	27	27	NA[d]	2	11	NA[d]
Test 2, run 2	870	20	20	NA[d]	2	12	NA[d]

[a]General temperature level for which differences apply. Differences may be either larger or smaller at other temperature levels.

[b]Between any two thermocouples employed in the test.

[c]Thermocouple 83 became unattached during run 1.

[d]Thermocouples not located on these cross sections in test 2; see Fig. 2.12.

and the infrared scan. Since the infrared scan represents the surface temperature averaged over the portion of the surface seen by the camera, circumferential variations tend to distort the axial distribution as recorded by the scan.

Visual observations of the bare heater tests indicate that the heater elongates approximately 16 mm over the temperature range of 20 to 930°C and approximately 19 mm over the range of 200 to 1200°C. Based on these data, the average coefficient of expansion for the heater assembly is approximately 20×10^{-6} mm/mm $°C^{-1}$ (11.1 in./in. $°F^{-1}$), which is essentially the same (as would be expected) as for the type 316 stainless steel sheath material.

Also, the freely suspended heater was observed to deflect laterally approximately 10 and 12 mm for the above temperature ranges. This deflection, which is induced by a circumferential temperature variation, was maximum in the region where PS-8, PS-9, and PS-10 burst. One would expect lateral deflection to occur in the simulator to the limit of the clearances permitted, causing local hot spots in the cladding.

Although interpretation of the bare heater tests is difficult and as yet, incomplete, the following observations can be made.

1. Temperature gradients in the heater, both axial and circumferential, increase with increasing temperature.

2. In the simulator, circumferential gradients in the heater tend to reduce the gas gap on the hot side (due to thermally induced bowing of the heater) and to increase the gap on the opposite side. The net effect is to accentuate the circumferential temperature variation in the Zircaloy tube during the transient.

3. These observations are consistent with results obtained in simulator tests in which this heater was used.

3. DEVELOPMENT AND PROCUREMENT

3.1 Component Development

J. L. Crowley

Fuel pin simulator lower end seal

The previous report[2] described a brazed assembly of ceramic insulators and metal fittings for the lower end seal of the fuel pin simulator. Although seals based on this concept are commercially available, unusual requirements placed on the simulator seal make it a special production assembly. An order was placed with the Ceramaseal Corporation for 20 of these special seal assemblies, with delivery expected in late January.

Meanwhile, a parallel investigation has been under way for an alternative design that might reduce the cost and delivery time. As a result, a second purchase order was placed with the same supplier for 20 seal assemblies of the alternative design. It is anticipated that the cost of these seals will be about half that for seals of the first design. Delivery of the second order is expected at the same time as the first. We will test and evaluate both designs for use in future simulators.

Requirements for the lower seal of the single-rod simulators are not as stringent as for the multirod bundles and can be met with standard electrical penetration seals.

Zircaloy tube-end adapter welds

In an effort to reduce assembly time, we investigated the feasibility of making the end adapter welds with the tungsten inert gas (TIG) process, using a local shield purged with argon instead of the special vacuum glove box method described in the previous report. Although the quality of the locally shielded weld is not as high as that obtained by welding in a glove box or by electron-beam (EB) welding, it is more than adequate for the short time exposure of the rod burst tests, and we are using the much

simpler welding process routinely in the fabrication of simulators. The welds are inspected visually and with liquid penetrant.

In addition to the investigation of welding techniques, we also evaluated a weld joint design that will improve alignment of the lower adapter with the Zircaloy tube. Improved alignment is important for the bundle test to facilitate assembly of the simulator through the close-fitting tubesheet at the upper end of the bundle.

Sample weld coupons were made using EB, dry box, and local shielding procedures and examined metallographically. Figure 3.1 shows the weld joint design, and Figs. 3.2 to 3.4 show examples of each type of welding procedure. All show excellent weld penetration and fusion, with no evidence of cracks. Porosity was observed in some of the TIG welds, but it was small, scattered, and isolated. The local-shielding procedure results in a higher level of contamination, causing an increase in hardness in the heat-affected zone. Since the simulators will be exposed to high-temperature steam for a few hours at most, proper care in setup and purging during the welding process will minimize contamination and the risks associated with slightly contaminated welds.

Examination of oxidized Zircaloy tubing

Prior to fabrication of fuel pin simulators, the Zircaloy tubing is pretreated in superheated steam [482°C (900°F)] for 30 min to produce a very thin oxide film on the inside and outside surfaces; details of the pretreatment process are presented in Section 5.

Specimens from two pretreatment runs were submitted for metallographic examination and evaluation.* Typical photomicrographs of the polished specimens are shown in Figs. 3.5 and 3.6. The specimen shown in Fig. 3.5 was taken from tube 645, which was pretreated in oxidation run 4, and the specimen shown in Fig. 3.6 was from tube 658 (oxidation run 5). The oxide film on each specimen was observed to be very thin (see Table 3.1) and surprisingly uniform considering the condition of

*Examination and evaluation were performed by R. E. Pawel, Metals and Ceramics Division.

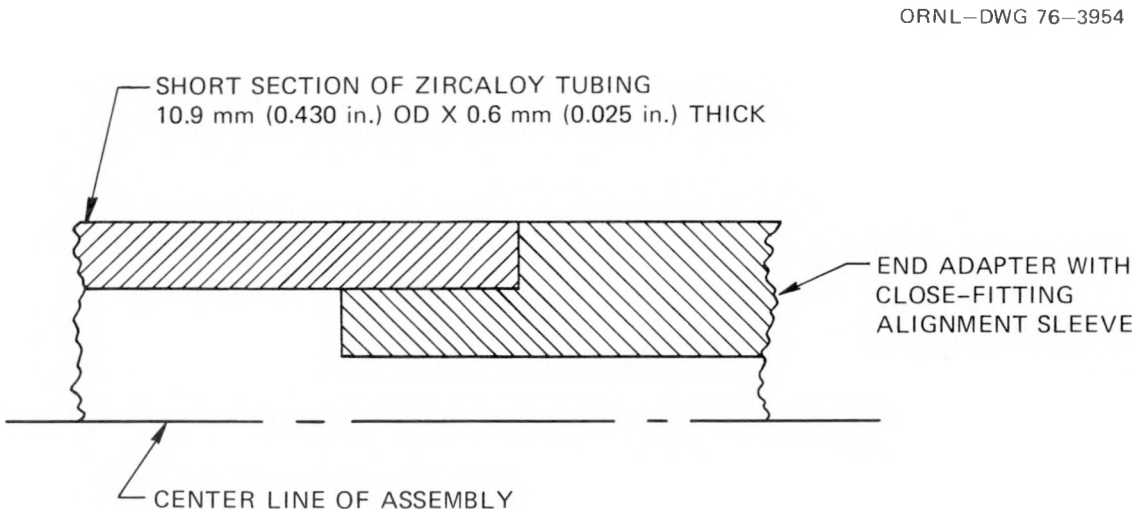

Fig. 3.1. Detail of lower end adapter weld joint.

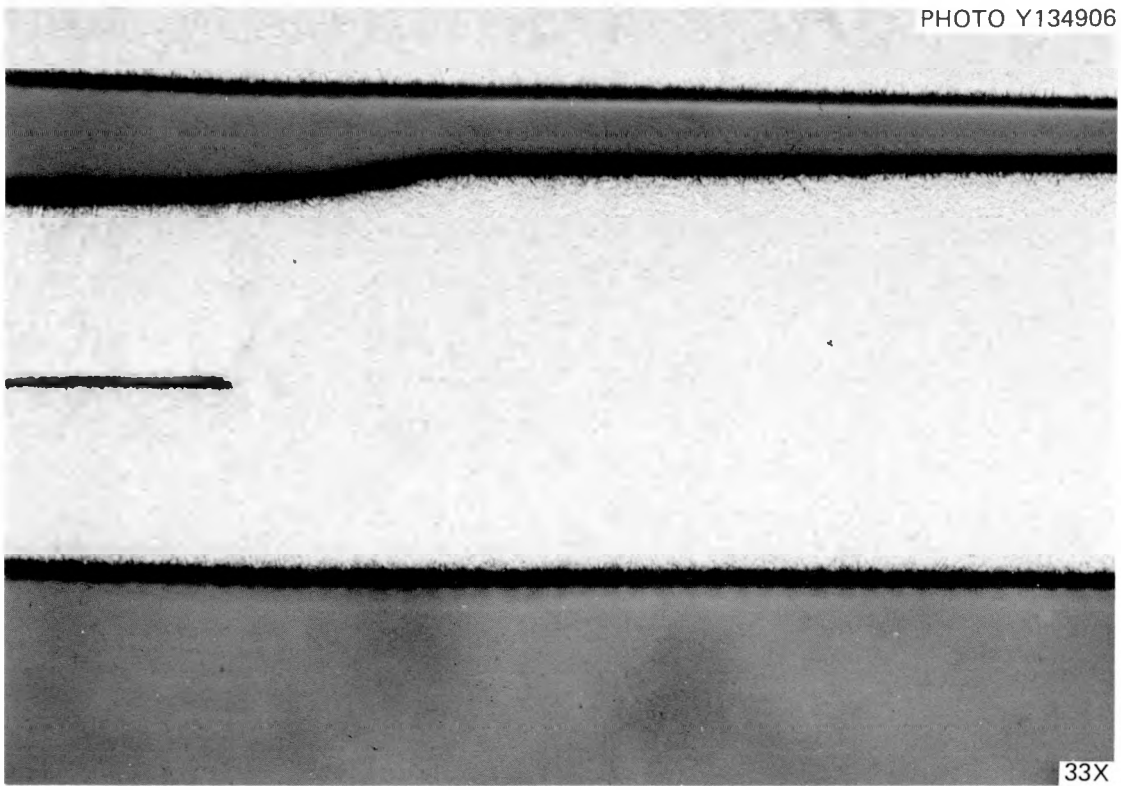

Fig. 3.2. Weld joint made by the electron-beam (EB) process (polished and etched; 33X).

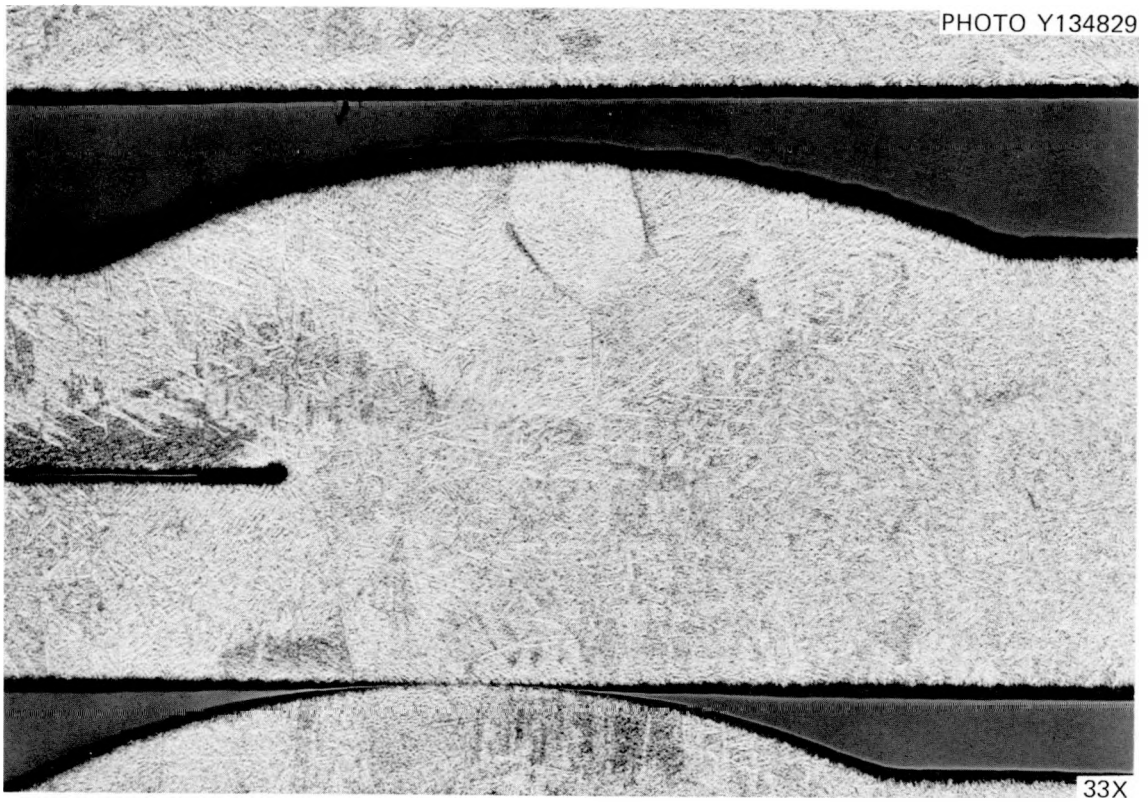

Fig. 3.3. Weld joint made by TIG process in dry box (polished and etched; 33X).

Table 3.1. Zircaloy tube hydrogen content and oxide film thickness

Tube No.	Condition	H_2 content (ppm)	Oxide thickness (μ)
645	Oxidized in 482°C steam for 30 min	33	1.5–2.0
658	Oxidized in 482°C steam for 30 min	35	0.5–0.7
634	As received	25	
307	As received	26	

Fig. 3.4. Weld joint made by TIG process with local shielding (polished and etched; 33X).

the original surface (as received) and the magnification of the photomicrographs.

Specimens from the treated tubes and from two tubes in the as-received condition were also analyzed for hydrogen. Results from the analysis are given in Table 3.1.

We conclude from this evaluation that the pretreatment given to the tubes prior to their assembly into simulators does not materially affect the metallurgical condition of the tubes, nor does it affect their performance during the burst tests. Of course, further oxidation will occur during the tests, and the amount can be determined during posttest examination.

Fig. 3.5. Photomicrograph showing oxide film produced on tube 645 during oxidation run 4 (as polished; 2000X).

3.2 Shroud Heating Tests

K. R. Carr* J. L. Crowley

The 16-rod square test array will be enclosed in a heated shroud fabricated from 0.24-mm-thick (0.0095-in.) Inconel sheet. Resistance

*Instrumentation and Controls Division.

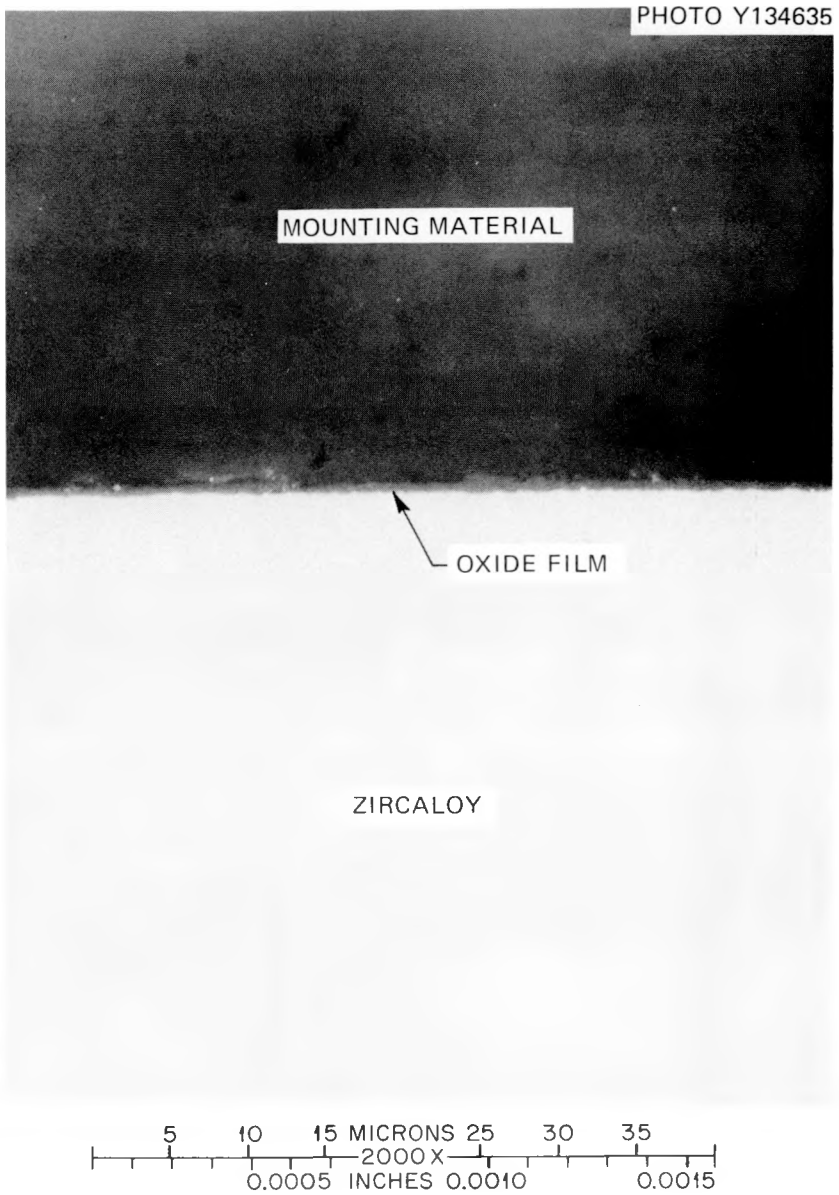

Fig. 3.6. Photomicrograph showing oxide film produced on tube 658 during oxidation run 5 (as polished; 2000X).

heating of the shroud is accomplished by connecting it (electrically) in series with the 16 parallel-connected fuel pin simulators. Adjustment of the shroud heating rate to match that of the fuel pin simulator [to maintain the two surfaces to within 55°C (∿100°F)] will be accomplished by varying the value of an external load resistance connected in parallel

to either the shroud or the bundle assembly. These selections must be established prior to the test.

Preliminary design calculations indicated that 11 to 12 kW of heater input power would be required to produce the desired simulator temperature ramp of 28°C/sec (50°F/sec); however, prototype simulator tests have shown that 9 kW of heater power is adequate. Thus, the shroud material is thicker than that needed to match the lower heating rate. Since the material has already been rolled and annealed for bundle fabrication and since a thinner shroud is undesirable, tests were conducted with a small strip of the shroud material to establish the load resistance needed to match the heatup rates within the stated limits.

The width of the strip was selected to represent a proportionate share of the total bundle power plus four additional heaters (in parallel with the bundle) acting as an external load resistance. Thus, while the bundle current would be that of 16 fuel pin simulators, the shroud current would correspond to that of 20 simulators. Results of the tests are shown in Fig. 3.7, wherein the temperature increase above room temperature is plotted as a function of time. Although this test began at room temperature and the burst tests will begin at approximately 343°C (650°F), the general relationship between shroud and bundle temperatures can be inferred. The nonlinearity exhibited by the shroud near the end of the transient is the result of the decreasing temperature coefficient of resistivity of Inconel and, perhaps, heat losses.

These tests also afforded an opportunity to investigate two different methods of making thermocouple junctions on the heated shroud. One type of junction, which we have used thus far in all our temperature measuring applications with the 0.25-mm-diam (0.010-in.) Pt vs Pt-10% Rh thermocouple wires, is made by spot welding the individual wires parallel to each other on the surface with a spacing of about 0.1 mm (∿0.005 in.) between the wires; this arrangement will be referred to hereafter as the "standard junction." Another type of junction is made by twisting the two wires and fusing them to form a small-diameter ball junction which is then spot welded to the surface; this arrangement will be referred to as a "ball junction."

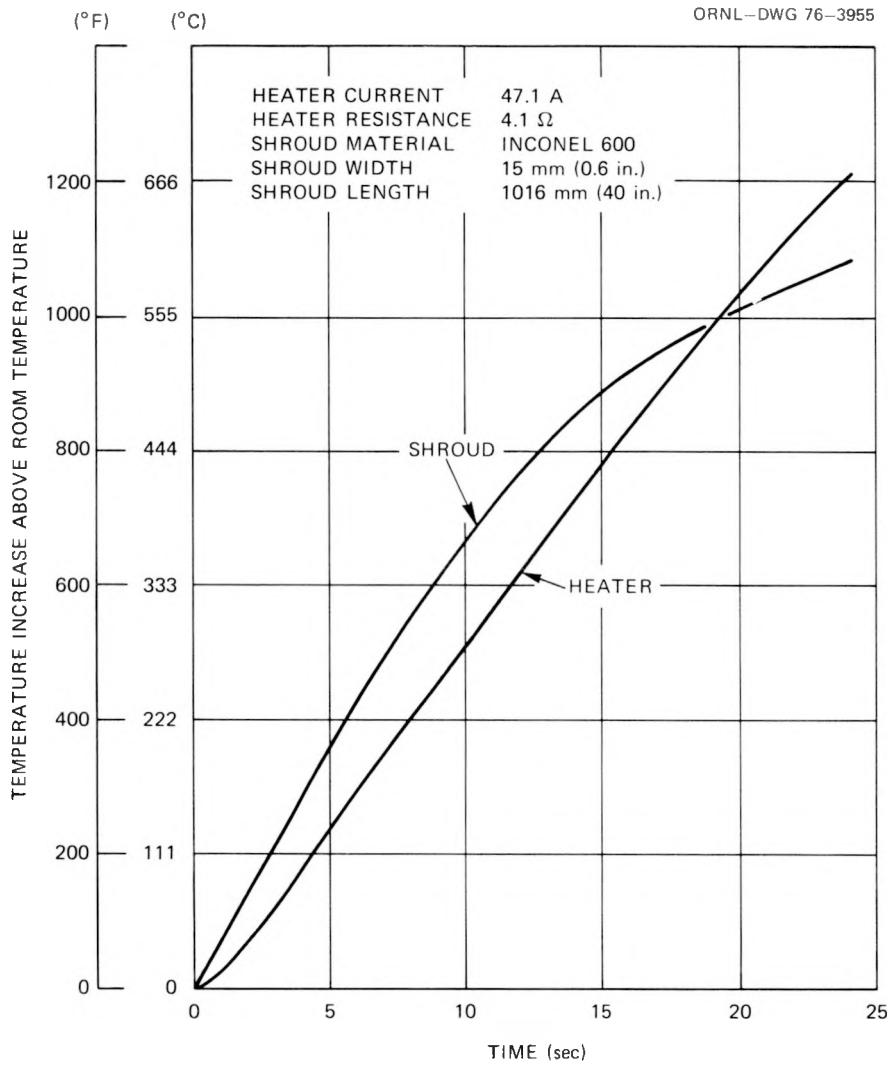

Fig. 3.7. Results of shroud heating tests.

As was discussed previously,[2] use of the standard junction on the current-carrying shroud may result in considerable error due to the voltage gradient imposed on the shroud. The ball junction, although having greater mass and perhaps slower response time, should eliminate the voltage gradient due to heating since the junction is located effectively at only one point.

Junctions of both types were attached to the heated strip (which modeled the shroud) and to the dummy load (a bare heater) in series with

the strip. The temperatures measured using this experimental setup are plotted in Fig. 3.7.

Based on these data, the following observations can be made.

1. The ball junctions completely eliminated the voltage gradient error in the shroud temperature measurements, but the standard junction thermocouples had voltage gradient offsets of as much as 445°C (∿800°F), that is, almost 5 mV.

2. Thermocouples with ball junctions located 50 mm (∿2 in.) apart on the shroud indicated the same temperature within 14°C (∿25°F).

3. The ball junction thermocouples had slower response times and lagged behind the standard junction thermocouples by as much as 33°C (∿60°F) in some cases, even though the sensing junctions were only 1.5 mm (1/16 in.) apart.

4. Thermocouples with small ball junctions appear to eliminate voltage gradient errors without introducing appreciable time delay errors in the shroud temperature measurements.

We are continuing to evaluate these results to determine an optimum method for installing shroud thermocouples.

3.3 Thermocouple Attachment Development

W. E. Baucum

As was discussed in the previous report,[2] nickel-plated stainless-steel-sheathed thermocouples can be satisfactorily welded to Zircaloy tubing using conventional spot welding equipment provided the Zircaloy is free of oxide. However, attempts to weld thermocouples to the inside surface of the tubing with the special welding apparatus developed for this purpose resulted in melting of the thermocouple sheath in the area in contact with the inner copper electrode. This problem was eliminated by machining a small radius (matching the thermocouple diameter) in the inner electrode to provide greater contact area on the sheath. Welds made with this electrode exhibited good tensile strength but were brittle and tended to break on flexing or twisting the thermocouple; spot welds made with the conventional equipment also exhibited these characteristics.

Tests were conducted with thermocouples having both tantalum (Ta) and nickel-plated stainless steel (Ni-SS) sheaths using different welding energies to maximize weld strength with minimum local deformation of the thermocouple and the Zircaloy tube. Energies of 50 to 70 Wsec and 40 to 60 Wsec, respectively, were found to be optimum.

We developed the following simulator assembly procedure for welding the thermocouples and inserting the heaters. The oxide film is first removed from the Zircaloy tubing at four small spots, located at the proper axial position and 90° from each other around the circumference, with a special oxide-removal tool. The tube is then placed over the special welding tool and carefully indexed to locate the thermocouples at the desired positions. Next, the thermocouples are inserted through the upper seal of the simulator and guided into the grooves of the welding tool. Each thermocouple is, in turn, placed in the radius milled in the electrode, the tube adjusted to the desired axial position, and the spot weld made. The tube is retracted from the electrode and rotated 90° to align the next thermocouple over the electrode. This sequence is repeated until all thermocouples are welded in place.

To protect and maintain thermocouple orientation, we use a grooved mandrel to push the welding tool out of the tube. The heater, which is grooved for the thermocouples and protected by a thin layer of plasma-spray-coated ZrO_2, is inserted into the lower end of the Zircaloy tube with its grooves properly oriented to accept the thermocouples and is pushed carefully through the tube, extruding the mandrel to complete the operation. The upper seal is then tightened to protect the internal thermocouples from further twisting or flexing.

Four thermocouples (two with Ta sheaths and two with Ni-SS sheaths) were spot welded to the inside of the Zircaloy tubing using the above procedure. Three of the welds broke during sliding of the tube and had to be rewelded. Welding energies for the Ta- and Ni-SS-sheathed thermocouples were 70 and 60 Wsec respectively.

The success achieved with spot welding nickel-plated stainless-steel-sheathed thermocouples suggested that a high-nickel-alloy sheath material might be better suited for this application. Consequently, an Inconel-sheathed thermocouple was obtained, and sample spot welds to the

Zircaloy tube were made with very encouraging results. The welds were very ductile and withstood higher tensile forces (before failure) than those made with nickel-plated stainless steel material. We are investigating the availability of Inconel-sheathed thermocouples for use later in the test program.

3.4 Thermocouple Procurement and Evaluation

T. G. Kollie*

Table 3.2 summarizes the procurement status of several types of thermocouples planned for use in the MRBT program. Thermoelements of item 1 are spot welded on the outside surface of the Zircaloy tubes to form an intrinsic thermocouple hot junction (called a standard junction in Section 3.2) and are expected to yield accurate measurements of the tube temperature. The sheathed thermocouples, items 2 to 5 and 7 to 8, will be used to obtain inside tube surface temperatures. The choice of sheath and thermoelement material for a given test will depend on the maximum temperature expected for that test. Item 6 thermocouples will be attached to the outside surface of several of the Zircaloy tubes in the No. 1 (4 × 4) bundle to augment the inside temperature measurements in a series of temperature mapping tests.

Serious difficulties encountered in manufacturing the tantalum-sheathed thermocouples (items 3, 4, and 5) have caused production delays and the cancellation of item 5. Items 3 and 5 were of identical design but from different manufacturers. Calibration and high-temperature evaluation tests were initiated on items 3 and 4 and on an alternate more easily fabricated thermocouple assembly consisting of an 0.125-mm-thick (0.005-in.) tantalum tube swaged over a standard 0.56-mm-diam (0.022-in.) stainless-steel-sheathed thermocouple. These tests will be completed next quarter.

A hermetic end seal was developed for item 6 using VA 508 glass frit manufactured by Vitrifunctions, Inc., Greensburg, Pa. The seal has been

---

*Instrumentation and Controls Division.

Table 3.2. Status of thermocouple procurement for MRBT Program

Item	Quantity	Type	Material		Diameter (mm)		Length (m)	Shipping Date	Comment
			Insulator	Sheath	Wire	Sheath			
1	Bulk material	S	Al_2O_3[a]		0.25		165	Received	Calibrated and in use
2	100	K	MgO	310 SS	0.10	0.75	3.28	Received	Calibrated and in use
3	95	K	Al_2O_3	Ta	0.10	0.75	3.28	12-23-75[b]	28 received; to be calibrated
4	10	S	Al_2O_3	Ta	0.10	0.75	3.28	12-23-75[c]	4 received; to be calibrated
5	25	K	Al_2O_3	Ta	0.10	0.75	3.28	Canceled	Manufacturer could not fabricate
6	60[d]	S	Al_2O_3	310 SS	0.25	1.60	2.46	Received	End seals and calibration to be made
7	50[e]	K	MgO	310 SS	0.10	0.71	3.28	3-1-76	Out for bids
8	50[e]	K	MgO	Inconel	0.10	0.75	3.28	3-1-76	Out for bids

[a] 1.60-mm-diam Al_2O_3 sleeve over bare wire.

[b] Original shipping date for 45 was 4-4-75; shipping date for the additional 50 was 12-1-75; delay by manufacturing difficulties; shipment of remainder (67) promised by 12-23-74.

[c] Original shipping date was 4-4-75; delayed by manufacturing difficulties; shipment of remainder (6) promised by 12-23-75.

[d] Bare-wire hot junction.

[e] Either item 7 or 8 will be ordered; includes option to purchase 50 additional thermocouples.

shown to be impervious to helium at 700 kPa (∿100 psi) at temperatures up to 482°C (900°F). At this temperature, the insulation resistance of the seal is much higher than that necessary to provide negligible electrical shunting of the thermocouple emf. The seal was cycled ten times between room temperature and 371°C (700°F) at rates of about 165°C/hr (300°F/hr) without failure; this heating rate is much higher than that to which the seal will be subjected in the burst tests. These seals are being installed on the item 6 thermocouples.

3.5 Heater Development and Procurement

W. E. Baucum R. W. McCulloch

R. W. McCulloch, one of our heater development specialists, visited RAMA and SEMCO during the period October 13 to 16 to aid in the resolution of heater fabrication problems. SEMCO has made progress in resolving fabrication difficulties; however, the heaters are not uniform in quality. New fabrication procedures to wind the heating elements are now being used, and preassembly inspection data on the coils and radiographs of the finished assembly both indicate improved uniformity. We expect smaller temperature variations (as indicated by infrared scans) in heater assemblies made in strict accordance with these new procedures.

RAMA has not yet demonstrated a capability for producing heaters in accordance with our purchase order requirements. A preproduction heater was received and scanned for surface heat flux uniformity (using the infrared technique) with unacceptable results. RAMA is of the opinion that the excessive temperature variation observed in the infrared scans of the heaters is due to poor crushing and recombination of the MgO core pieces, which results in poor thermal contact between adjacent cores and between the MgO core pieces and the heater coil. The preproduction heater was sectioned and examined to determine if this is the case. Although a few interfaces were observed between adjacent MgO core pieces, crushing and recombination appeared to be generally good. Also, there appeared to be very good contact between the cores and heater coil as evidenced by adherence of the MgO to the inside surface of the coil. The spacing between coil turns, which is related to coil heat

generation, was also measured and appeared to correlate well with the infrared scan. Thus, these results indicate that variation in the heater coil spacing was the principal cause of the variation in the sheath temperature. Since infrared scans of an as-wound coil (from RAMA) indicated unusual uniformity in heat generation along its length, the coil was probably upset during subsequent fabrication by either the filling and tamping operation or the swaging operation. Both local differences in the as-filled annular BN density and variations in MgO core hardness can lead to coil damage during the swaging operation.

RAMA is continuing attempts to fabricate a heater that fully meets our purchase order specification and will not attempt production of heaters until the fabrication problems are resolved. Until acceptable uniformity is demonstrated, it is meaningless to speculate on heater delivery schedules from this supplier.

As mentioned in the previous report,[2] a new concept of heater fabrication, which involves the use of cold-pressed BN preforms instead of the conventional powder fill, is being investigated. Three prototype heaters were fabricated (two by SEMCO and one by RAMA) in cooperation with ORNL heater development personnel. These heaters were swaged lightly [0.25 mm (0.010 in.) diametral reduction] after assembly. However, infrared scans showed large sheath temperature variations (as much as 70% of the average temperature), indicating poor thermal contact within the assembly. The heaters were reswaged at ORNL to reduce the diameter by an additional 0.25 mm (0.010 in.). Subsequent scans showed remarkable improvement in all three heaters. The RAMA heater, which had the greatest initial variation before reswaging, showed the most improvement, that is, a reduction in temperature variation to 13%. The heaters will be swaged further in an attempt to reduce the variation to acceptable levels, that is, 10%. Also, RAMA attempted to fabricate a heater using cold-pressed BN preforms for the core and BN powder filling for the annular region outside the heating coil. The core preforms broke during the tamping of the powder in the annular region, creating voids in the central core. Use of core preforms with higher densities might solve this problem.

During this report period, we received an additional 21 heaters from SEMCO, for a total of 30, and 1 heater (discussed above) from RAMA, for

a total of 11. Of the 30 SEMCO heaters, 7 were judged to meet the original specifications; 7 were purchased as being of potential use, although they did not quite meet the specifications; 10 did not meet specifications but were purchased at a reduced price for evaluation and scoping tests; 4 were rejected outright, and 2 were specially fabricated, using BN preforms, for evaluation purposes. Of the 11 RAMA heaters, 2 met the purchase order requirements; 8 did not meet specifications but were bought for evaluation and scoping tests; and 1 was rejected. The infrared scanning test on as-received heaters was the major differentiating factor in determining their quality.

From the performance to date, it is clear that SEMCO is the only vendor capable of producing heaters acceptable for the MRBT test program. For this reason and because of the press of program schedules, a decision was made to exercise an option for 40 additional heaters from SEMCO, even though the original order for 20 heaters was not complete (6 remain to be delivered). This should minimize the delay between the completion of the initial heater order and the beginning of delivery of the subsequent order. However, SEMCO has not yet accepted the option and has indicated the desire for some contractual changes before accepting it. This will be fully discussed with the SEMCO representative, who will be visiting ORNL in the early part of January 1976. Until these matters are resolved, delivery of additional heaters remains uncertain.

4. DESIGN, FABRICATION, AND CONSTRUCTION

4.1 Mechanical Design

J. L. Crowley H. R. Payne*

Several drawings were revised during the quarter to correct errors and/or to improve the design concept. With these revisions, all the mechanical design drawings needed to permit testing 4 X 4 bundles are complete and in the shops for fabrication.

4.2 Electrical Design

J. L. Crowley R. D. Stulting* M. D. Trundle*

Electrical design drawings of the dc power supply modifications, ac power controls, and electrical details and equipment layouts were revised to reflect changes needed to permit satisfactory operation and coordination with the Thermal-Hydraulic Test Facility (THTF). Eight revised drawings showing as-built changes, added ground detectors, instrument power changes, and additional shell heaters and thermocouples, and one new drawing showing steam line heater details were issued. Design changes needed to permit increased shroud current by addition of a variable-load resistance in parallel with the test bundle will be initiated next quarter.

4.3 Instrumentation and Controls Design

K. R. Carr† C. S. Meadors*

Design drawings of the instrumentation and controls system were completed and issued for fabrication and assembly. The design includes components and wiring details to permit testing of both 4 X 4 and 8 X 8 bundles; however, installation at this time will be limited to wiring

---

*General Engineering.

†Instrumentation and Controls Division.

and components necessary for the 4 X 4 bundles. Major features of the design are given below.

Temperature measurement. Thermometry is achieved primarily with thermocouples referenced to a 65.5°C (150°F) datum. "Universal" reference junctions, which are stable to within ±0.08°C (0.15°F), permit the use of either type K (Chromel vs Alumel) or type S (Pt vs Pt-10% Rh) thermocouples in the facility. Signals from the thermocouples will be recorded by the computer-controlled data-acquisition system (CCDAS) for subsequent millivolt-to-temperature conversion with appropriate polynomials.

Thermocouples that are spot welded to the inside surface of the Zircaloy tubes will be 0.75-mm-diam (0.030-in.) metal-sheathed type K or S, depending on the maximum temperature expected in a particular test. The sheath material will be either tantalum or nickel-plated stainless steel, again depending on the expected temperature level. A number of 1.5-mm-diam (0.060-in.) stainless-steel-sheathed type S thermocouples will be used to measure the temperature of the shroud surrounding the bundle. These thermocouples will have the sheath removed (and sealed to prevent entry of moisture) to expose the thermoelements for several centimeters. Sensing junctions will be formed by spot welding the exposed wires to the shroud. Signal-isolation amplifiers will be used to protect the CCDAS from the high common mode voltage of the electrically heated shroud.

A platinum resistance thermometer is provided in the bundle steam inlet to permit independent verification of proper functioning and pretest checks of the bundle thermocouples.

Pressure measurement. Steam pressure in the test vessel and helium pressure in each of the fuel pin simulators will be measured with strain-gage-type, Wheatstone-bridge pressure transducers located on a manifold adjacent to the test bundle. In-situ calibrations of the pressure transducers will be made with a secondary-standard Bourdon-tube-type gage having an accuracy of ±14 kPa (2 psi) over the range 0 to 14,000 kPa (0 to 2000 psi). Zero-offset and span-calibration constants for each transducer will be stored in the data system. In this way, the transducer signals can be input directly to the data system rather than via signal

conditioners, which are often used to provide zero and span corrections for this type of transducer. This approach permitted significant savings (about $27,000 for the 8 X 8 array) in the cost of signal conditioners.

Control circuits. The operator controls for the facility are on two panels, a control/status panel located in the THTF control room adjacent to the CCDAS and an auxiliary control panel located in one of the three instrument cabinets near the test bundle. The control circuits, together with the CCDAS, provide for three types of tests (verification, thermal mapping, and rod burst) and four modes of test termination as described previously.[2]

The control/status panel will be mounted to permit operator monitoring of an existing THTF cathode-ray tube (CRT) display. The CRT can be used to display up to 100 data channels as vertical bar graphs side by side with heights proportional to the magnitude of the respective individual channels. With proper grouping of selected channels, this readout will provide the operator with an easily interpreted general overview of the progress of an experiment.

Physical features. With the exception of field-mounted instruments and the existing data system, the instrumentation and controls for the 4 X 4 rod array tests will be housed in three standard instrument cabinets located in the vicinity of the test bundle and in the operator's control panel in the THTF control room. Space is provided for a fourth standard instrument cabinet for mounting additional thermocouple reference boxes that will be needed in the future for the 8 X 8 rod array tests.

4.4 Data Acquisition and Software

K. J. Cross*

The analog input system of the CCDAS has undergone extensive evaluation and testing due to indications of system digitization error exceeding

---

*Instrumentation and Controls Division.

the nominal specification of 0.3% of full scale. The digitization error was apparently introduced by one or more of the following:

1. signal offset due to voltage offsets and/or leakage in the switching FETs,
2. an error due to the recovery time of a saturated amplifier,
3. an error caused by channel-to-channel interaction,
4. an error due to reduced common mode rejection ratio (CMRR).

The error mechanisms were characterized by diagnostic experiments in which observed errors correlated well with calculated predictions.

The recovery time of the programmable-gain amplifier subsystem from "hard" saturation to within specifications is on the order of 100 msec and can influence subsequent readings when sampling at a rate of 10,000 readings per second. Since the recovery time is inherent in the design, it is necessary to arrange the scan table so that the signal ranges (gain) specified for each channel are sufficiently wide to preclude amplifier saturation under any expected condition. Also, during pre-test instrument checkouts, malfunctioning instruments that would cause an open circuit ("soft" saturation) must be corrected or bypassed.

The offsets due to voltage drops across switching or leaky FETs are peculiar to individual eight-channel multiplexor cards or to single channels on a card. This effect can cause a maximum error up to 200 μV referred to input (RTI). A test box is used off line to check multiplexor cards for leakage and to adjust for voltage nulls across the FETs. This is then followed by several on-line (in-circuit) tests. A procedure is being prepared to specify the checkout and adjustment operations. These checks are to be performed periodically but not necessarily prior to each test run.

An offset of up to 20 μV RTI has been observed when signals of greatly different levels are scanned consecutively. Both this channel-to-channel interaction and a reduction in the CMRR are directly attributable to the single-pole RC filters at the input of each FET multiplexor channel. These effects can be minimized to an insignificant level by properly constructing the scan table. This generally includes the scanning of a shorted channel between channels that might interact with each other.

Several additional features have been added to the CCDAS to enhance its capabilities for collecting data and to generate quick-look summaries. However, due to projected CCDAS use by other projects, the generation of quick-look summaries is being transferred to the ORNL large-scale computer systems. Work is under way on software programs to produce various print-outs and plots to aid in the analysis of the data.

4.5 Fabrication and Construction

J. L. Crowley

Construction activities during this report period included the installation of switchgear, fuse racks, and interconnections of the dc power system to the THTF, and the provision of ac power for auxiliary heating. Shop fabrication of the helium pressurization system is complete, but field assembly has not been initiated. Progress was made on fabrication of the bundle test components. A shortage of manpower, due to the heavy work load associated with the checkout and operation of THTF, has slowed assembly of the bundle test equipment. The THTF effort will decline drastically early next quarter, thereby permitting increased effort for the MRBT test facility. Since the test bundle determines the test schedule, these delays are not expected to create a significant impact.

4.6 Multirod Bundle Assembly Procedure

J. L. Crowley

The bundle assembly procedure, a critical requirement for the proper assembly of a test bundle, is in its third writing. A preliminary procedure was supplied by the mechanical design group; this was expanded and rewritten in the proper form for a sign-off-type assembly procedure. All comments on this draft by design, quality-assurance, and operations personnel have been collected and integrated into a third draft. Detailed procedures for the attachment of bare-wire and sheathed thermocouples are yet to be written.

5. OPERATIONS

5.1 Single-Rod Test Facility

J. L. Crowley

The versatility designed into the test facility permits tests of various types to be performed with minimum modifications. This capability is reflected by the types and number of tests conducted (see Table 5.1) in the facility this quarter.

Maintenance during the quarter was minor, consisting mostly of repairs and improvements to the instrumentation.

The task of fabrication and assembly of fuel pin simulators has become more routine to the craftsmen and technicians, enabling them to suggest improvements in technique, quality, and assembly time. Detailed procedures are prepared for use with each assembly. Although many of these are similar, variations in heaters, spacers, thermometry, end seals, etc., require careful attention to each assembly procedure.

5.2 Zircaloy Tube Oxidation

J. L. Crowley

During this report period, a total of 35 Zircaloy tubes were oxidized in the oxidation autoclave to produce a thin film on both the internal and external surfaces of the tubes. As many as seven tubes can be oxidized in a run. The oxidation process involves electrically heating the autoclave to 482°C (900°F) while supplying superheated steam at 482°C (900°F) and atmospheric pressure at a flow rate of about 12.5×10^{-4} kg/sec (10 lb/hr). These conditions are maintained for 30 min after equilibration. Total time in the steam atmosphere includes 2 to 3 hr heatup time, 30 min at stable conditions, and 2 to 3 hr cooldown time. The results of metallographic examination of two typical specimens are discussed in Section 3.1.

The oxidization runs and the Zircaloy tubes oxidized during this report period are listed in Table 5.2.

Table 5.1. Tests conducted this quarter in the single-rod test facility

Test No.	SEMCO heater	Simulator gas volume (cm^3)	Thermocouples		Remarks
			External	Internal	
PS1-6	Prototype 2	26.3	21	0	To study temperature distribution
PS1-7	Prototype 2	26.3	21	0	To study temperature distribution
PS1-8	Prototype 2	26.3	21	0	To study temperature distribution
PS1-9	Prototype 2	26.3	21	0	Burst test
PS-10	S/N 2828005	35.8	8	0	Burst test; standard test transient
PS-11	S/N 2828005	37.1	8	0	Modified test transient; no burst
PS-12	S/N 2828006	41.3	33	0	To study temperature distribution and burst
PS-13	S/N 2828005	34.5	8	0	Modified test transient; no burst
PS-14	S/N 2828006	41.4	8	0	Burst test
PS-15	S/N 2828006	46.8	12	3	Evaluate internal thermocouple performance
PS-16	S/N 2828005	37.8	8	0	Burst test at high pressure; test aborted
BH5-1	S/N 2828005	NA	14	NA	To study heater temperature distribution
BH5-2	S/N 2828005	NA	10	NA	To study heater temperature distribution
BH1-1	Prototype 1	NA	14	NA	To study heater temperature distribution
SH-1	Prototype 2	NA	5	NA	Shroud heating test
SH-2	Prototype 2	NA	5	NA	Shroud heating test

Table 5.2. Zircaloy tubes oxidized this quarter

Run No.	Zircaloy tube numbers						
5	648	649	650	657	658	659	660
6	285	292	298	301	304	311	662
7	287	290	293	303	306	652	664
8	286	289	299	302	305	651	663
9	288	291	294	300	310	661	668

5.3 Steam Flow in Single-Rod Tests

J. L. Crowley

Steam flow for the single-rod burst tests is estimated from condensate collected at the outlet of the test vessel. Since steam leakage occurs (intentionally) around penetrations in both the upper and lower closure flanges, the measured amount is not an accurate indication of the flow through the test vessel. To be exact, leakage around the lower flange penetrations should be added to the measured flow, but leakage around the penetrations in the upper flange does not pass through the vessel and should not be considered. The upper leakage should be much greater than the lower leakage, since all the thermocouple penetrations (no effort is made to seal them) are located in the upper flange.

Normally, the measured steam flow in the burst tests is in the range of 4 to 6 $\times$ 10^{-4} kg/sec ($\sim$3 to 5 lb/hr). A special test was conducted to determine if significant error was being made in the measured flow. The flow test was conducted with temporary flanges attached to the test vessel to eliminate leakage. Since the pressure in the vessel is essentially atmospheric, the supply pressure (downstream of the control valve) represents the pressure drop through the system; this pressure is adjusted to

the same value for each burst test. With this pressure setting, the measured steam flow in the "no-leakage" configuration was 9.4×10^{-4} kg/sec (7.2 lb/hr), a factor of about 1.5 to 2 greater than the normally measured value, that is, 4 to 6×10^{-4} kg/sec (3 to 5 lb/hr). Since most of the leakage is through the upper flange penetrations (and never passes through the vessel), the normal value (4 to 6×10^{-4} kg/sec) represents the flow through the shroud tube with sufficient accuracy.

REFERENCES

1. *Quarterly Progress Report on Reactor Safety Programs Sponsored by the Division of Reactor Safety Research for July–September 1974*, ORNL/TM-4729, Vol. I, pp. 70–72.

2. R. H. Chapman, *Multirod Burst Test Program Quarterly Progress Report for July–September 1975*, ORNL/TM-5154.

ORNL/NUREG/TM-10
NRC-1, -3

Internal Distribution

1. W. E. Baucum
2. M. Bender
3. C. J. Borkowski
4. J. R. Buchanan
5. K. R. Carr
6. J. V. Cathcart
7-21. R. H. Chapman
22. N. E. Clapp
23. W. E. Cooper
24. W. B. Cottrell
25. K. J. Cross
26. J. L. Crowley
27. F. L. Culler
28. B. G. Eads
29. G. G. Fee
30. M. H. Fontana
31. M. J. Goglia
32. R. A. Hedrick
33. R. E. Helms
34. D. O. Hobson
35. H. W. Hoffman
36. G. Hofmann
37. A. F. Johnson
38. T. G. Kollie
39. R. E. MacPherson
40. A. P. Malinauskas
41. W. R. Martin
42. W. J. McCarthy
43. R. W. McCulloch
44. D. L. McElroy
45. C. S. Meadors
46. C. A. Mills
47. R. L. Moore
48. F. H. Neill
49. H. R. Payne
50. H. Postma
51. J. P. Sanders
52-53. M. R. Sheldon
54. I. Spiewak
55. R. D. Stulting
56. J. J. Taylor
57. D. G. Thomas
58. D. B. Trauger
59. J. R. Weir
60. G. D. Whitman
61. W. J. Wilcox
62. Patent Office
63-64. Central Research Library
65. Document Reference Section
66-70. Laboratory Records Department
71. Laboratory Records (RC)
72. Nuclear Safety Information Center

External Distribution

73. M. P. Bohn, Aerojet Nuclear Company, Idaho Falls, Idaho 83401
74. J. R. Larson, Aerojet Nuclear Company, Idaho Falls, Idaho 83401
75-82. Director, Division of Reactor Safety Research, Nuclear Regulatory Commission, Washington, DC 20555
83. Director, Reactor Division, ERDA, ORO
84. Director, Research and Technical Support Division, ERDA, ORO
85-390. Given distribution as shown in categories NRC-1 and -3 (25 copies to NTIS)

☆ U.S. GOVERNMENT PRINTING OFFICE: 1976-748-189/328